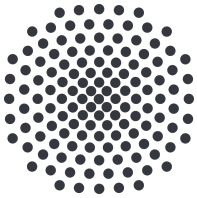

University of Stuttgart

SoSe 23

DLR Design Challenge 2023

PERSEUS - Post-Emergency Response and Surveillance UAV System

Anil Abhishek (3518094)

Hennemann Alexander (3634460)

Kimmel Hellen (3388237)

Mayer Christian (3633584)

Müller Lukas (3388703)

Reischl Tobias (3634512)

Submitted:
11.07.2023

Supervisor:
M.Sc. Johannes Schneider
Prof. Dr. Andreas Strohmayer

Universität Stuttgart

Institut für Flugzeugbau

Institutsleitung
Prof. Dr. Peter Middendorf
Prof. Dr. Po Wen Cheng
Prof. Dr. Andreas Strohmayer

Universität Stuttgart
Institut für Flugzeugbau • Pfaffenwaldring 31 • **70569 Stuttgart**

Kontakt
Johannes Schneider
Pfaffenwaldring 31
70569 Stuttgart
T 0711 685-60483
F 0711 685-62449
E-Mail:
schneider@ifb.uni-stuttgart.de
www.ifb.uni-stuttgart.de

Betreff: Bestätigungsschreiben

06.07.2023

Sehr geehrte Damen und Herren,

hiermit bestätige ich, dass die im Folgenden aufgeführten Mitglieder des studentischen Teams selbstständig den Flugzeugentwurf und Bericht zur Teilnahme an der DLR-Design Challenge 2023 durchgeführt haben.

- Abishek Anil
- Alexander Hennemann
- Christian Mayer
- Hellen Kimmel
- Lukas Müller
- Tobias Reischl

Mit freundlichen Grüßen,

Johannes Schneider

Betreuender wissenschaftlicher Mitarbeiter

Abstract

This design study discusses an innovative configuration of a blended-wing body aircraft as a next generation high altitude emergency service unmanned aerial vehicle. The technical implementation is hereby presented and evaluated, with special emphasis placed upon a sustainable propulsion system as well as efficient aerodynamics. Furthermore, an operating concept and fleet system is outlined. Additional areas of application with different payloads are shown. This design was developed in the context of the DLR Design Challenge 2023 with a fixed Entry Into Service (EIS) in 2040. The analysis shows that in the near future, an aircraft powered by a sustainable propulsion system can be used for fast and safe restoration of communications as well as radar surveillance. It is shown that a sustained flight time of 17 hours in 18 km height is achievable and a substantial cost reduction and improved flexibility is possible compared to satellite-based systems.

In dieser Arbeit wird eine innovative Konfiguration eines Blended-Wing Bodies als ein hochfliegendes unbemanntes Luftfahrzeug der nächsten Generation entworfen. Dabei wird die technische Umsetzung vorgestellt und bewertet, wobei ein besonderer Schwerpunkt auf einem nachhaltigen Antriebssystem und effizienter Aerodynamik liegt. Darüber hinaus wird ein mögliches Betriebskonzept und Flottensystem dargelegt. Weitere Einsatzgebiete mit unterschiedlichen Nutzlasten werden aufgezeigt. Diese Arbeit wurde im Rahmen der DLR Design Challenge 2023 für einen festgelegten Entry Into Service (EIS) in 2040 entwickelt. Die Analyse zeigt, dass in naher Zukunft ein Flugzeug mit einem nachhaltigen Antriebssystem zur schnellen und sicheren Wiederherstellung der Kommunikation sowie zur Radarüberwachung eingesetzt werden kann. Es wird gezeigt, dass eine kontinuierliche Flugzeit von 17 Stunden in 18 km Höhe erreichbar ist und im Vergleich zu satellitengestützten Systemen eine verbesserte Flexibilität und Kostenreduktion möglich ist.

Picture of Team members

Anil Abishek

- M. Sc. Student - Aerospace Engineering
- 4th Semester
- Powertrain and Thermal Management

Hennemann Alexander

- M. Sc. Student - Aerospace Engineering
- 3rd Semester
- Fleet concept and Operation

Kimmel Hellen

- M. Sc. Student - Aerospace Engineering
- 1st Semester
- Autonomous Systems and Flight Control

Mayer Christian

- M. Sc. Student - Aerospace Engineering
- 3rd Semester
- Transportation, Ground Station and Cost

Müller Lukas

- M. Sc. Student - Aerospace Engineering
- 2nd Semester
- Aerodynamics and Propulsion

Reischl Tobias

- M. Sc. Student - Aerospace Engineering
- 3rd Semester
- CAD and Structure

Contents

List of Figures

List of Tables

List of Symbols

A	Lifting area	$[m^2]$
C_D	Drag coefficient	[-]
C_{D0}	Zero drag coefficient	[-]
C_L	Lift coefficient	[-]
$C_{L_{loit}}$	Lift coefficient during loiter	[-]
D_{loit}	Drag during Loiter	[N]
e	Oswald factor	[-]
g	Gravity acceleration	$[\frac{kg}{m \cdot s^2}]$
L	Lift	[N]
L/D	Lift over Drag	[-]
m_{LH_2O}	Mass liquid water	[kg]
m	Mass	[kg]
m_{LH_2O}	Mass flow liquid water	$[\frac{kg}{s}]$
m_{Tank}	Mass tank	[kg]
p_t	total pressure	[Pa]
$P_{Battery}$	Battery power	[W]
P_{cruise}	Cruise power	[W]
P_{loit}	Power during loiter	[W]
P_{VTOL}	Vertical takeoff Power	[W]
$\dot{Q}$	Rate of heat flow	[W]
R	Gas constant	$[\frac{J}{kg \cdot mol}]$
T_t	Stagnation temperature	[K]
v_{loit}	Loiter speed	$[\frac{m}{s}]$
ρ	density	$[\frac{kg}{m^3}]$
η_{EDF}	Efficiency during loiter	[-]
Λ	Aspect ratio	[-]
$\frac{\dot{m} \cdot \sqrt{R \cdot Tt}}{A \cdot p_t} = 0.45$	Dimensionless mass-flow parameter	[-]
μ_{Tank}	Mass fraction tank	[-]

List of Abbreviations

ADS-B	Automatic Dependent Surveillance - Broadcast
AI	Artificial Intelligence
AoA	Angle of Attack
AOA	Angle of Arrival
ATC	Air Traffic Control
BWB	Blended Wing Body
C2	Command and Control
CA	Collision Avoidance
CAD	Computer Aided Design
CFD	Computational Fluid Dynamics
DAA	Detect and Avoid
DLR	Deutsches Zentrum für Luft- und Raumfahrt
DOC	Direct Operating Costs
EDF	Electric Ducted Fan
EIS	Entry Into Service
FSO	Free Space Optical
GNSS	Global Navigation Satellite Systems
HALE	High Altitude Long Endurance
HAP	High Altitude Platform
HIDS	Host-based Intrusion Detection System
IMA	Integrated Modular Avionics
IMU	Inertial Measurement Unit
LiPo	Lithium Polymer
MGS	Mobile Ground Station
MRO	Maintenance, Repair and Overhaul
PCM	Protection Circuit Module
PEM	Proton Exchange Membrane
RSS	Received Signal Strength
RTD	Resistance Temperature Detector
RTK	Real Time Kinematic
RWC	Remain Well Clear
SST	Shear Stress Transport
STM	Surveillance and Tracking Module
TDOA	Time Difference of Arrival
TOA	Time of Arrival
TRM	Threat Resolution Module
UAV	Unmanned Aerial Vehicle
VOR/DME	VHF (very high frequency) Omnidirectional Range/Distance Measuring Equipment
VTOL	Vertical Take-Off and Landing

1 Introduction

In today's interconnected world, the seamless and reliable provision of Internet and mobile communications has become an indispensable requirement for a well-functioning society. Despite significant progress, however, even highly developed economies such as Germany still face the challenge of maintaining uninterrupted service, especially after natural disasters such as floods and severe storms. But it is precisely in such situations that reliable and uninterrupted communication is essential to coordinate rescue forces and organize assistance. In such situations, a system is needed that is capable of establishing communications as quickly as possible while also providing area-wide radar surveillance. Satellite-based systems already exist that can provide widespread Internet coverage. However, these systems involve immense costs, are not sustainable and generate dependency on other states and companies. Therefore, a system of interconnected and intelligent drones should be developed that can be deployed flexibly and operated sustainably.
In the following, Team PERSEUS from the University of Stuttgart presents a possible implementation of such a system, which is to be put into operation in 2040. Special attention is paid to sustainable technologies that will be available in the future. In particular, the sustainable propulsion system, realized by a hydrogen fuel cell, is not feasible at this time. Therefore, intensive literature research was carried out to get an overview of the current state of research as well as the expected developments, especially in the field of the power density of fuel cells, to validate the assumptions made for 2040. Another key technology is VTOL capabilities, which give the system great flexibility. In addition to this, an operational concept has been developed. Like the Greek god Perseus who rescued Andromeda from danger and freed his mother, the PERSEUS UAV system helps humanity by restoring communications in disaster and emergency situations.

2 Rated Concepts

2.1 Scenarios and Requirements

The design challenge specifically includes two scenarios that must be covered by the developed concept. In scenario 1, Internet communications must be restored in Hamburg (755 km^2; 1,854,000 inhabitants) and Schleswig-Holstein (15,804 km^2; 2,922,000 inhabitants) after a large-scale outage. The aircraft must be able to fly 100 NM from the base station to the deployment site and also return and land. During this mission, another emergency, scenario 2, occurs at a distance of 170 NM. Radar surveillance must be initiated in a circular area of 700 km^2 within less than 2h. In addition, Internet connectivity must be restored. Both scenarios must be permanently covered.
The overall objectives are to minimise costs, emissions and time to restore Internet connectivity. In addition, the fleet must be operational up to the 55th latitude. Entry into service (EIS) is scheduled for 2040.
The requirements are summarized and listed in table 2.1.
An Internet relay, an antenna system for the relay module, a radar system and an antenna for communication with the ground station are specified as black boxes.

No.	Requirement
1	Fly 100NM from base station to site of operation
2	Restore Internet in Hamburg and Schleswig-Holstein
3	Return to base station and land
4	Travel 170 NM in less than 2h
5	Provide Internet and radar surveillance for 700km^2
6	Cover scenario 1 and 2 permanently
7	Fleet deployable up to 55th parallel
8	Entry into service in 2040

Table 2.1: Requirements

2.2 Preliminary design process

After an initial estimate of how many UAVs would be needed to cover the area specified by the task, the decision was made to develop a high-altitude aircraft concept to minimise the number of vehicles needed. For manned aircraft, labour time must be considered and pilot costs must be paid. Also, many additional systems such as pressurized cabins for high altitudes, cockpits, or survival equipment are required. For this reason, an unmanned solution was chosen. A market survey showed different approaches for this flight altitude like balloons, airships, high-altitude long endurance (HALE) military drones or solar-powered aircraft (figure 2.1). Since balloons and airships are not capable of meeting requirement 4, these approaches were eliminated.

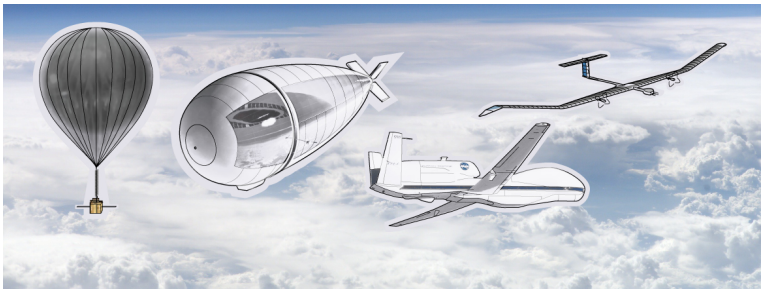

Figure 2.1: Existing Concepts [12]

Solar aircraft are difficult to operate year-round at latitude 55 (requirement 7). Since the shortest day at this parallel is about 7 hours of daylight [65], operating an aircraft on solar power would require a large area covered with solar panels and heavy battery system, which does not seem feasible. To meet today's sustainability requirements, other green energy sources such as fuel cells, batteries and super capacitors were evaluated according to criteria such as thrust, power, mass, consumption, size, efficiency, attainable speed and maintenance complexity. The concepts were scored for each criterion, which was weighted to reflect its importance in the final result. To cover the different energy and power requirements of all flight phases, a hybrid system consisting of all three technologies was chosen. This power train system is described in 3.7.
Several propulsion units were considered: Jet engines, electric propellers and combustion engines. Following a similar evaluation process as for power sources, electric propellers were selected.
To enable PERSEUS to operate from any location at any time, VTOL capabilities were implemented. In addition, a transport system based on standard truck trailers was developed, which also serves as a mobile ground station. This allows the UAVs to take-off and land independently of airport infrastructure or road bases.
There are several approaches to realizing VTOL capabilities: Two different propellers for VTOL and normal flight, each optimized for its task, or only one type for both phases of flight. In this case, since the VTOL time is small compared to the total mission time, only one type of tilt propellers is used to save dead mass and reduce drag during flight.
Several configurations have been discussed, such as a classic aircraft configuration, canards and Blended-Wing Bodies (BWB). The advantage of the BWB is its aerodynamic performance. Due to the smaller wetted area, the skin friction is reduced and the interference drag is lower [105]. In addition, the disadvantages normally associated with a BWB are not significant for unmanned designs. The mass disadvantage due to a non-circular pressure hull and the reduced passenger comfort due to a windowless cabin are not applicable [105]. For this reason, a BWB concept was chosen. To improve stability and allow vertical take-off anywhere and anytime, the drone was equipped with a canard.

3 Aircraft Concept

Taking into account the various requirements listed in section 2.1 and the design process, it is now necessary to design a good fuselage around the given payloads such as the radar, antenna, internet relay and rod antenna.
The following design was chosen as the most appropriate for the given scenario and will be explained in more detail below.

3.1 Overview

In short, the primary objective of this concept was to create an aircraft that could cruise at the desired altitude for as long as possible. To achieve this, it has to produce as much lift as possible, while minimising drag as much as possible. Because of the very long loitering phases, this can only be achieved by a wing with a high aspect ratio and a body shaped like an airfoil to produce more overall lift. Due to the fact that it is an unmanned design and only carries a payload in the form of electronic components, the most appropriate shape to achieve this objective is essentially a BWB concept, as discussed in chapter 2.2.
To tackle the drawback of reduced steering authority due to the missing tail unit at the rear of the fuselage, the precise control of the rotation speed of the Electric Ducted Fans (EDF) is used for differential steering. The EDFs are placed on top of the ailerons, both at the wing and canard, to achieve yaw authority.
Since this concept takes off completely vertically and does not roll on a runway, a conventional landing gear is not required, primarily to save mass and maintenance work. Instead, both canards are fitted with a rubber cap at the lower end and integrated shock absorbers to withstand the remaining loads in the event of a rough touchdown. At wing level, two additional retractable legs extend out from the fuselage for stabilization and to stand on.
The technical drawings and resulting dimensions are shown in figure 3.1 - 3.3.

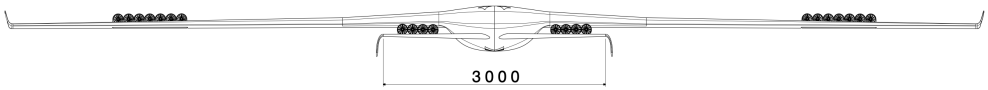

Figure 3.1: Front View [mm]

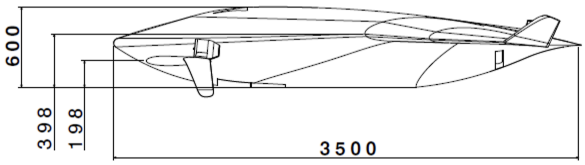

Figure 3.2: Side View [mm]

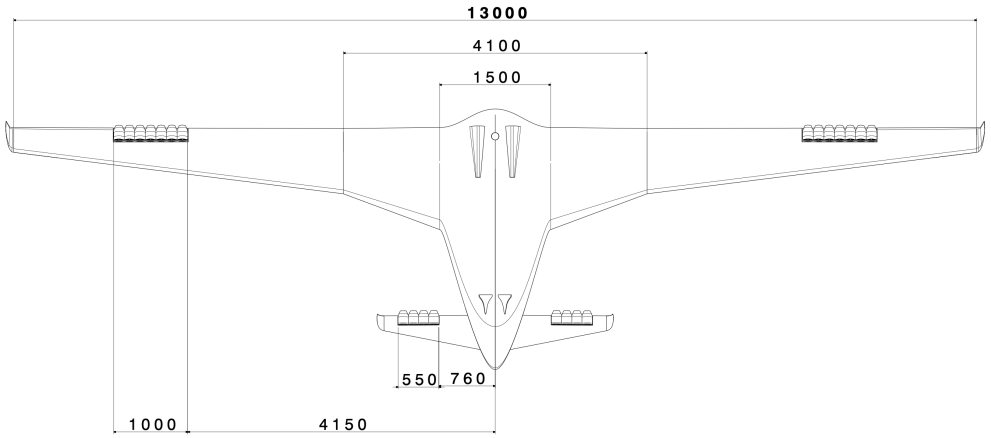

Figure 3.3: Top View [mm]

To also maintain a high flexibility in deployment, that is discussed in more detail in section 4.3, the high aspect ratio wing must be fitted with a modular concept. Figure 3.4 shows the separation of the wing into three different parts, for storage in a container box that will be discussed in 4.3.
To allow for even more flexibility for later use cases, the payload area of the UAV for the Internet and radar module (red cube in figure 3.4) is also featured with a modular concept to allow for fast exchange when being on ground or the truck station. This allows for an easy switch of any payload that fits the size of the Internet relay that measures 500 x 250 x 250 mm (L x W x H). This idea will be discussed in more detail in section 4.2.

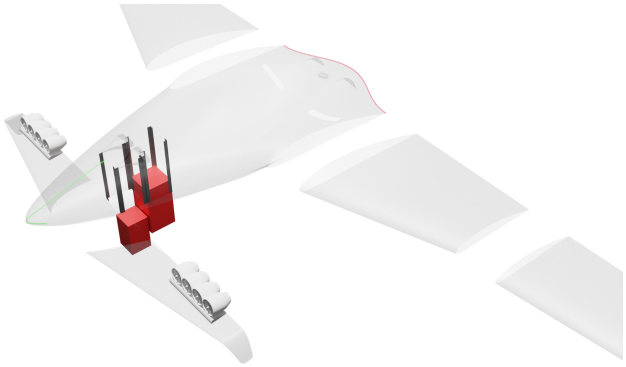

Figure 3.4: Modular Concept

3.2 Key Technologies and Arrangement

With all the necessary specifications for the design and the most suitable technologies to fulfil them identified, it is imperative to amalgamate these components into a viable concept. Figure 3.4 shows the final configuration of the UAV. When placing the components, not only the final mass of the concept, but also soft factors like maintainability and thermal management were considered. Table 3.1 list the key technologies and their current and predicted readiness level.

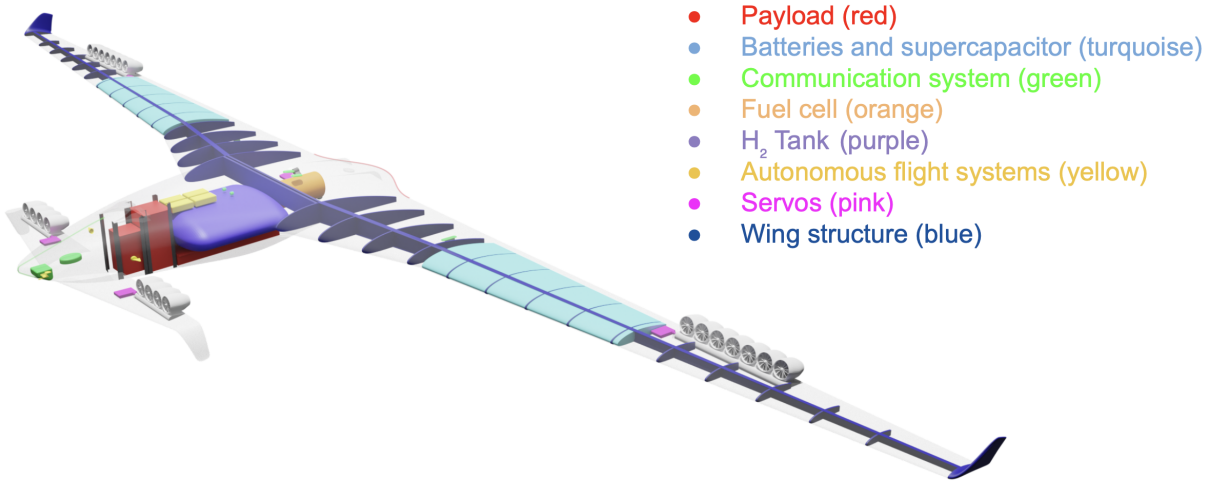

Figure 3.5: Internal arrangement of components

Technology	Readiness Level (2023)	Readiness Level (2040)
Modularity	8-9	9
Fuel cell in very high altitude	3-4	7
Battery and supercapacitor	3-4	8
Fully autonomous operation	6	9
VTOL capability	7	9
Blended wing body design	6	8-9

Table 3.1: Key Technologies

3.3 Preliminary Sizing

Now that a final concept has been selected, preliminary sizing must be carried out, followed by more detailed calculations once the exact dimensions of the UAV are known, to confirm that the performance requirements will be met.
In the usual preliminary sizing process, empirical data is used to obtain an estimation of the expected maximum takeoff mass of the aircraft. This assumption is based on mission parameters like the payload mass, required range, configuration of the aircraft, etc. Like all data-driven processes, this sizing method tends to become more accurate when more data on aircraft operating with similar parameters is available. This is where traditional sizing approaches fail for PERSEUS because there are almost no aircraft operating at a similar combination of very high altitude and very small payload. While loitering UAVs for similar altitudes exist, these are mostly used in a military context and have a takeoff mass an order of magnitude larger than expected for our design. Moreover, the process is further complicated by the EIS with the date being set as 2040, adding further uncertainty to traditional sizing methods by extrapolating statistics of old airplanes into the future.
Therefore, a component-based mass estimation process was chosen, where the mass of each component is estimated based on mission and aircraft parameters. For example, the size and mass of an engine can be estimated by the power it must provide, which in turn can be calculated if the expected aerodynamic efficiency of the aircraft is known. This process is subject to uncertainty, but it does make it easier to incorporate informed estimates of future performance for each component, based on current research in the respective fields.
As variable design parameters for our preliminary sizing, the lift coefficient $C_{L_{loit}}$ during loitering and the total lifting area A were chosen. Therefore, a system of equations modelling the mass and performance of the aircraft based on these parameters must be obtained. The aircraft was sized to sustain 20 hours of loitering at operation altitude if climb and return home were omitted. So its final duration at target will be slightly shorter.
As a result of the preliminary sizing process, a map of the minimum achievable takeoff mass for each combination of the design parameters was obtained. For all calculations, the mass of the aircraft was assumed to be constant. Although the stored hydrogen is consumed during operation, this effect has been ignored due to its small mass fraction. Furthermore, although multiple payload configurations are used, all calculations have been made for the worst-case configuration of two communication boxes, both in terms of mass and power consumption.

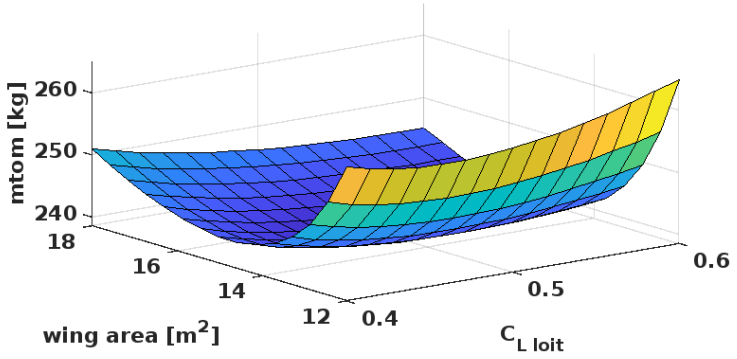

Figure 3.6: Results of the preliminary sizing process

Since the map shown in figure 3.6 does not consider soft factors such as storage, transportation and handling by ground crew, a design point slightly off the minimum mass was chosen with an area of 12.5 m^2 and a lift coefficient of 0.47. With the preliminary masses and sizes, the final design was created and verified to achieve the required performance. To avoid confusion, the values obtained during preliminary sizing will only be shown in their respective section. The final masses can be found in table 3.4 and the final performance is shown in table 3.5. Both can be found in the last section of this chapter.

3.4 Aerodynamics

The overall goal is to create an aircraft that is as aerodynamically efficient as possible. Therefore, the wings are optimized for the dominating flight phase while fulfilling the restrictions imposed by the remaining flight phases. A good example of such a constraint on classical aircraft design is the maximum landing speed imposed by regulations [22], requiring the installation of complicated and heavy high-lift devices.
For PERSEUS design, the dominating flight phase for which the wing will be optimized is loitering at altitude. A major difference from typical, cruise-optimized aircraft is that the optimization objective changes from minimum energy required for a given distance to minimum energy required for a given time in flight. This moves the optimum design point to a lower flight speed. The power demand during loitering can be calculated as

$$P_{loit} = \eta_{EDF} * \frac{m * g}{L/D_{loit}} * v_{loit} \tag{3.1}$$

[69] and scales linearly with the loitering speed. During horizontal flight the lift generated must match the weight of the UAV, therefore the loitering speed can be calculated with

$$v_{loit} = \sqrt{\frac{2 * m * g}{\rho * C_{L_{loit}} * A}} \tag{3.2}$$

It follows that for optimal performance during loitering, a large wing with a high lift coefficient and L/D would be optimal. Aircraft that perform well in these parameters are gliders and the UAV will have similar long, unswept wings with a high aspect ratio. Since the shape of the body is not imposed by requirements like pressurisation or a large payload, it will be designed to work as a lifting body, further increasing aerodynamic efficiency. Furthermore, the canard configuration allows fulfilling the momentum balance while generating lift, adding to the efficiency of the design. Because it generates lift, the canard should be modelled as a separate wing. However, due to its relatively small size, the added complexity of the preliminary calculations was not considered worthwhile. It was therefore decided to use the total floor area of the aircraft as the reference area for all calculations, treating the entire aircraft as one large wing.
To estimate the L/D of the aircraft, the drag coefficient must be modelled. The drag acting on a wing can be separated into parasitic drag caused by friction and induced drag caused by trailing vertices that are a direct result of generating lift[44]. Since the aircraft is modelled as one big wing, interference drag can be omitted and the drag coefficient can be modelled as

$$C_D = C_{D0} + \frac{C_L^2}{e\Lambda\pi} \tag{3.3}$$

To assume the Oswald factor, aspect ratio and parasitic drag from the wing area, a preliminary estimation of the wing shape must be made.
The shape and area of the centre body are governed by the payload and other components and are assumed to be independent of the wing area. As shown in 3.7 the shape of the wing was chosen as a trapezoid, a compromise between ease of manufacturing and lift distribution [9]. With the assumed dimensions, the wingspan and therefore aspect ratio becomes a function of the lifting area. The Oswald factor was assumed to be 0.85 following textbook methods [87].
To obtain a full overview of the wing's design space, the parasitic drag C_{D0} must be calculated. This can be done with sufficient accuracy for preliminary sizing by treating the aircraft skin as a flat plate. Flying at low Reynolds numbers, the flow over the wing is assumed to be laminar, while the flow for the lifting body is assumed to be turbulent. With these assumptions, a parasitic drag coefficient can be calculated with textbook methods [87]. Using all these equations, the aerodynamic performance can be estimated as a function of the preliminary design parameters.

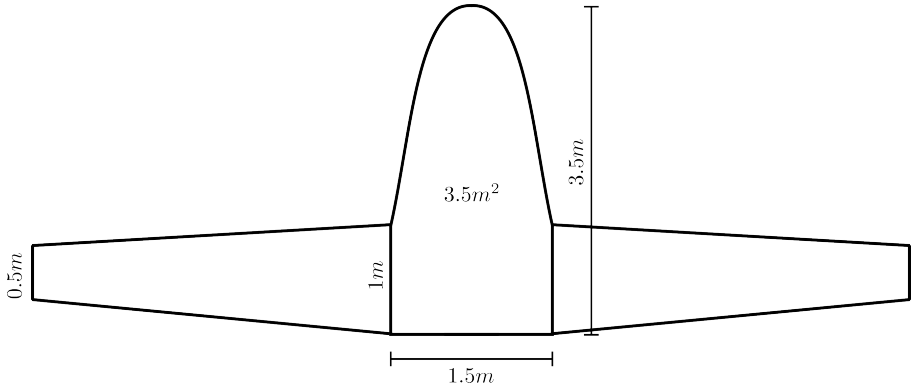

Figure 3.7: Floor plan assumed for preliminary sizing

As mentioned before, secondary requirements like a maximum landing speed can limit the aerodynamic design space. However, due to the VTOL capability, this limitation does not apply since high-lift capabilities are not required. Laminar airfoil design is very attractive because of its low drag. This decoupling of horizontal flight from take-off and landing is therefore very beneficial, as these profiles can suffer from laminar flow separation when operating at high lift coefficients and low Reynolds numbers. The VTOL configuration eliminates this problem.
As noted above, laminar profiles will be used to reduce the friction drag on the wings. Furthermore, active laminar flow technologies were considered but not deemed beneficial for our design because of their energy consumption and added mass and complexity.
Additionally, a morphing wing design was considered because of its possible drag reduction. These mechanisms allow for a change in local lift without requiring a sectioning of the wing. This is achieved by adapting the shape of the airfoil shell itself and not changing the relative locations of wing sections like classic control surfaces do. Therefore, the airflow around the airfoil is not disturbed, resulting in less drag [61]. However, these mechanisms offer only a limited range of motion and are therefore unfit to be used for control surfaces carrying the EDFs, since a tilt of over 90° must be realized to ensure full control during VTOL. While the main wings could be fitted with two control surfaces each, a classic one for VTOL and a morphing one for control during normal flight, the increase in cost, mass and complexity was not deemed worth it. Therefore, a morphing wing was omitted and classic control surfaces were used.
To further reduce the induced drag at low speeds, winglets were added. While adding more wingspan is generally more mass efficient, winglets become attractive when considering the difficulty in handling large wings.
In the final configuration, the placement of the main wing and canard relative to the centre of gravity must fulfil multiple requirements. Canard and wing will be vertically separated so that the trailing vortex of the canard does not impact the wing, resulting in a loss of lift and momentum imbalance. To achieve static stability around the pitch axis, the main wing must be placed behind the centre of gravity far enough to out-leverage the canard. Finally, the canard is sized so that flow separation occurs before the main wing stalls. This layer of safety is not strictly necessary for an autonomous vehicle, but welcome.
Since the aircraft lags a horizontal stabilizer and rudder, stability and control of the yaw axis are achieved through differential thrust and an active control system.
For the loitering conditions, the preliminary sizing predicted an L/D of 24.77 with a lift coefficient of 0.47. This performance was validated with a CFD calculation in OpenFOAM. The calculation was done at operating altitude and rhoSimpleFoam was used as a solver, simulating a compressible flow using an SST k-omega turbulence model. For a production design, the wing would be designed using a full inverse process, but this is outside the scope of this challenge. Therefore, the design was only optimized according to the Prandtl lifting-line theory using the Aero 5 tool [2]. Since the exact EDF geometry is unknown they were omitted from the simulation, the same was done with internal airflows. These uncertainties must be considered when evaluating the calculated results.
As a result of the CFD calculations, an L/D of 25.8 was found. Subject to the uncertainties mentioned above, this result strongly indicates that the design L/D will be achieved.

3.5 Structure

The aircraft is built as a composite sandwich structure due to the high performance offered concerning mass. Since the UAV operates both in normal flight and VTOL, the different load characteristics of these flight phases must be considered, keeping stresses and deformations at an acceptable level.
The main body is a monocoque design, whereas the wings feature a one-beam construction with evenly spaced ribs, as shown in figure 3.8. The ribs to which the control surfaces carrying the propulsion system are attached to must be reinforced. This is because during VTOL, those ribs transfer all the load to the wing beam, which in turn must be able to support the load as well. In addition, the ribs where the wing is divided for stowage must be dimensioned for this purpose.

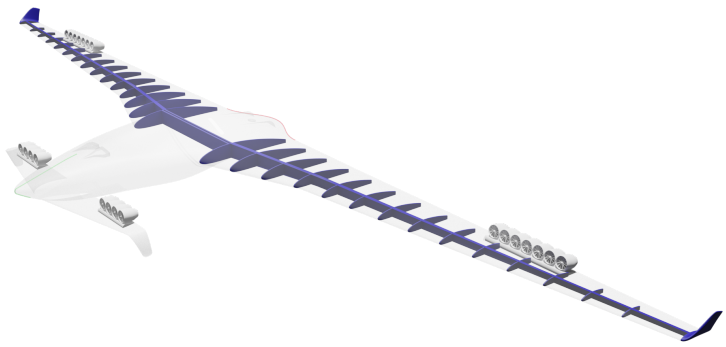

Figure 3.8: Overview of the load bearing wing structure

Because the aircraft carries components that rely on emitting and receiving radiation, the areas where these components are located cannot be built using conductive materials.
To ease inspections and maintenance, in places where it is beneficial, the half shells will be split further. Detachable bindings with minimal aerodynamic impact are used for assembling. Therefore, these panels can be easily taken off to access the components underneath, providing adequate working conditions for inspections and maintenance. This reduces not only the associated work time and costs, but also ensures a quick turnaround time and high readiness of the fleet.
Since for the mission at hand the UAV only starts and lands in VTOL, the landing gear does not support horizontal takeoff or landing. It is mainly designed to absorb the shock when landing vertically while being as light as possible. However, a modified version to operate the UAV from classic runways can be easily implemented because of enough space inside.
To estimate the resulting mass of the structure, the area mass density of the sandwich structure used in construction was assumed to be 1 kg/m^2, a conservative assumption based on [78].
Since the final shape of the aircraft was not known during the preliminary sizing, it was assumed that the area of the shell was linearly dependent on the total lifting area. Besides the beam was of constant size with a length equal to the total wingspan calculated according to 3.7. Furthermore, to account for smaller sub-assemblies and mounting hardware, a multiplication factor of 1.2 was assumed to estimate the final mass of the structure.
For the parameters chosen in preliminary sizing, a structural mass of 66.3 kg was calculated. For the final design, the mass could be calculated more accurately using the total surface area obtained from CAD. However, the factor of 1.2 was retained to account for the missing sub-assemblies. As a result, the final mass of the structure, including the landing gear, was calculated to be 63.2 kg.
High-risk areas of the outer shell will be reinforced to further increase impact tolerance [17]. In addition, if the technology is demonstrated, incorporating piezoelectric sensing fibres into the structure will provide valuable data for the predictive maintenance algorithm [20]. Additionally, in places where electric heating is deemed the most viable option e.g. air intakes, heating elements will be embedded into the laminate [16].

3.6 Propulsion

The Propulsion system must be capable of serving two very different flight states, the VTOL phase with its high thrust requirements and the loitering phase where low thrust at a high altitude is required.

Designing a highly detailed propulsion system with a known rotor geometry is outside the scope of this challenge. However, the parameters that are important for the aircraft design process – mass, size and power consumption – can be estimated with sufficient accuracy.
Although splitting the propulsion system into two subsystems, each dedicated to a phase of flight would facilitate optimization, it would impose significant aerodynamic and mass penalties, which were not considered acceptable. There are designs that do not suffer aerodynamic penalties, such as propellers that are mounted in the wing and covered during flight [90], [33]. However, these systems require complicated mechanisms that add additional failure points and mass.

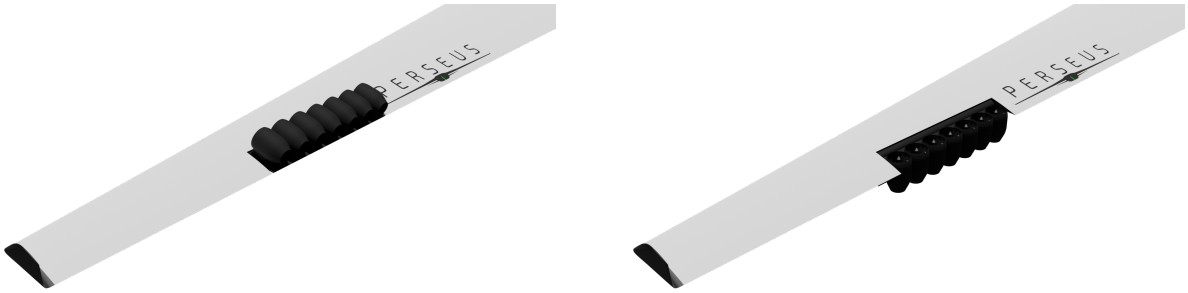

(a) Flight phase (b) VTOL Phase

Figure 3.9: Control surface in normal flight and VTOL

As shown in figure 3.9, EDFs are mounted on control surfaces with enough range of motion to serve in VTOL and normal flight. While EDFs have advantages over open propellers, like a reduction in noise level and a stator row to unswirl the outflow, increasing efficiency, the main reason that favours EDFs is the additional protection of the ground crew. On one hand, the casing prevents direct injuries that occur when body parts interact with the rotor. On the other hand, it contains not only a blade-off, but also prevents any foreign objects that are ingested from being flung towards personnel standing nearby.
While some technical improvements in the field of rotor design and motor technology are expected until 2040 they are projected to be minute in comparison to progress that will be made in other technologies relevant to our design. A promising technology, especially for configurations that use liquid hydrogen as power supply, are superconductor based systems, where the low-temperature hydrogen is used as coolant [71]. However, for the low constant power requirements of the mission, the additional mass, cost and complexity of such a system is unlikely to be viable. Therefore, this technology is not explicitly considered, but might be implemented if the technology develops accordingly.
Since the thrust demand of the VTOL phase is about an order of magnitude larger than in normal flight, the VTOL phase was identified as the defining flight phase for the sizing of the propulsion system. While basic estimations for the power consumption during VTOL can be made using the disk theory, the results underestimate the real power demand [82]. This approach was deemed too inaccurate and as the expected improvements in mass and power are small, data sheets from existing EDFs were used to estimate the size, power requirements and mass of the propulsion system. As a result, it was assumed that for every kilogram of mass, the VTOL system could provide 78.48 N of thrust while operating at optimum efficiency, resulting in a power consumption of 44.85 W per Newton of thrust. While the ground effect might reduce the actual power demand, it could not be modelled sufficiently and was therefore ignored.
The system has been designed to provide the thrust required for a steady hover with optimum efficiency, so it is able to provide more thrust albeit it while operating at lower efficiency, which is required for climb and transition to normal flight. Since the propulsion system is oversized regarding normal flight, it can be assumed that it can provide the required thrust for loitering even at high operating altitudes.
An alternative approach has been taken to calculate the power requirement during cruise and loitering, using an equation 3.1 based on the derivation of the Breguet range equation for turboprop aircraft.
For all calculations, the EDFs efficiency is assumed to be $\eta_{EDF} = 0.8$. While in reality this value varies with flight conditions and EDF geometry, this assumption is reasonable for preliminary sizing, since it was assumed that the blade geometry is optimized for the two dominant flight phases, loitering and VTOL.
For the final configuration, the mass of the propulsion system was calculated to be 37.5 kg, with a power demand of 110 kW during VTOL and 10.24 kW while loitering at 18 km.
The placement of the fans has a major impact on control authority. To balance the momentum along the pitch axis, there are 4 fans on each canard and 7 on each side of the wing. Roll authority is provided

by placing the EDFs away from the centre line. It's a balancing act, as placing them further apart gives better roll control, but this becomes a disadvantage if the thrust of the EDFs doesn't match up in normal flight, or if one of the EDFs fails. Furthermore, it increases the bending moment on the wing root during hover but reduces the bending moment during normal flight. All these factors must be considered when choosing the distance to the centre line.
While in configurations such as quadcopters the yaw authority is relatively small compared to the other axis, in this configuration the EDFs are tilted to achieve superior control in the VTOL phase. Since the design features no classical vertical stabilizer, differential thrust is used to control the yaw axis during normal flight [18].
Failure modes in the different flight phases were considered and since the propulsion system is designed to operate with thrust reserves in all flight phases, failures of individual components can be tolerated [57].

3.7 Hybrid Power Train

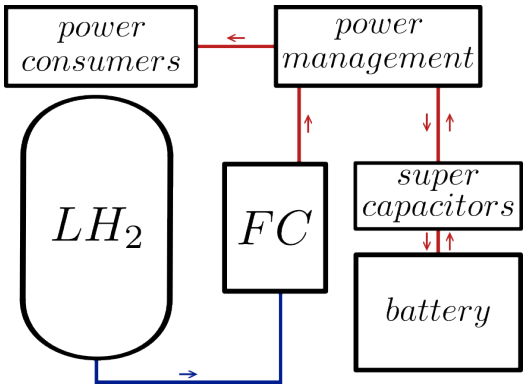

Figure 3.10: Powertrain sketchup

An outline of the power train is shown in figure 3.10. It is based on two power sources: hydrogen and battery power. While the hydrogen-based subsystem was chosen because of its high gravimetric energy density for long missions, the battery subsystem was chosen for its high gravimetric power density. Oversimplified, it could be said that the battery system is used to supply the VTOL phase and the hydrogen system supports normal flight. However, because of their unique synergy effects, both systems are useful in VTOL and normal flight.

3.7.1 Battery System

In most existing and planned electric propulsion aircraft designs, the batteries are used for sustained flight phases and therefore the gravimetric energy density is the determining factor for sizing. This is also the case in the automotive industry, where gravimetric energy density limits the current range of electric vehicles. As the automotive industry is one of the main driving forces behind battery development [83], a lot of research is focused on increasing this energy density, while power output is more of an afterthought. However, in the design presented here this is fundamentally different, as the battery system is only used for a short duration where a high power output is needed. Therefore, the gravimetric power density is the limiting factor.
To predict the power output required from the battery system during VTOL, a few assumptions are made. Firstly, the fuel cell operates at its maximum possible power output, which is assumed to be double the power output when loitering at altitude, the reason for which is described later in section 3.7.2. Since some power is required for climbing it is assumed, that the battery system must provide the power required to hover minus 50% of the fuel cells power output, resulting in $P_{Battery} = P_{VTOL} - P_{cruise}$.
Among the currently available battery types, lithium polymer batteries were identified as the best fit for this purpose, specifically those used for small drones. Since the life expectancy of these batteries is diminished at higher C-ratings, the acceptable C-rating during VTOL is limited to 25C. When currently available lithium polymer batteries were analysed, a gravimetric energy density of 160 Wh/kg was found. As mentioned earlier, most research and therefore predictions of future performance have focused on high energy density batteries. Since lithium polymer batteries are a derivative of lithium-ion batteries, it is deemed reasonable to project the expected performance increases onto lithium polymer (LiPo) technology. The FutPrInt50 Project predicts an energy density of 600 Wh/kg for Li-Ion batteries in 2040 [30] with the current energy density at 250 Wh/kh. This is an increase of 140 %. To keep the estimate conservative, it is assumed that the resulting increase in energy density for LiPo technology is around 100 % and the energy density of a 25 C lithium polymer battery is predicted to be 300 Wh/kg in 2040. This leads to a gravimetric power density of 7.5 kW/kg, with which the mass of the battery system can be predicted. Assuming the maximum depth of discharge acceptable would be 75 %, the battery system could support VTOL for 108 seconds, which is enough for takeoff and transition into vertical flight. To predict the size

of the battery system, the density of currently available 25C batteries was analysed and calculated to be 2 kg/l; this value was also used to predict the size of the battery system.
For the final design, the battery mass was calculated to be 13 kg, providing 97.5 kW of power during VTOL at a system size of 26 litres. Since the battery system is located in the wing of the aircraft, where a lot of space is still available, eventual changes in the size of the systems do not pose a problem. Electronics needed to support the battery operation are considered as a constant mass.
During normal flight, the role of the battery system changes from that of a main power source to that of an energy buffer, so the electronics must be able to charge the batteries with the electrical energy produced by the fuel cell. Since fuel cells have a slow response to changes in power demand, the battery system is used to make up the difference, as discussed in section 3.7.2. Furthermore, the battery system increases the effective service sealing of the aircraft, which is limited to an altitude at which the required climb rate of 0.5 m/s can be achieved [10] by providing excess power to perform an evasive manoeuvre even when the fuel cell is operating at maximum power. In addition, it adds redundancy to the power train, since the battery can sustain flight controls and communication in case the fuel cell fails, allowing the aircraft to glide or even cruise at low power to an adequate position for an emergency or controlled crash landing.
Since the temperature of the batteries during discharge has a significant impact on the expected lifetime [27], the battery system must include a temperature control system to maintain the batteries at an acceptable temperature during all phases of flight. It must therefore be capable of cooling and heating the batteries. Furthermore, the use of super capacitors has been shown to improve battery life expectancy by covering very short duration spikes in power demand [94], so these will be used to minimise battery degradation. Since the temperature control systems requires temperature sensors, the data generated by these will be used for the predictive maintenance system to estimate the remaining lifespan of the batteries.
The recharging time of the battery system affects the turnaround time of each aircraft and depends on the discharge depth of the batteries. Assuming the average landing time will not exceed 60 seconds and the batteries were fully charged by the fuel cell when the landing process begins, the batteries will be discharged by 42 %. Since the temperature of the cells during charging seems to affect the build up of lithium depositions at the anode [13], one of the main driving factors of degradation, the charging rate must be limited. The charge time is estimated at around 10 minutes, which would result in an acceptable average charging rate of 2.5 C.

3.7.2 Fuel Cell

The fuel cell is the main power plant of the aircraft and is sized to deliver the constant power required while loitering at altitude, which consists of the power required by the propulsion system, the payload and secondary systems.
One of the biggest challenges is the operating conditions at a loitering altitude of 18 km, where the outside air has a temperature of -57 °C and a density that is only 1/10 of that at sea level. Therefore, the reaction air provided to the fuel cell must be treated to create adequate operating conditions.
While some research has been done on the operation of fuel cells at altitude [102] and some aircraft designs incorporating them are currently being worked on [91], these are systems that are sized for power outputs an order of a magnitude higher than expected for our design. However, their systems can be adapted to our use case, especially since [102] designed a system to operate at 18 km of altitude. However, the mass estimations can not be transferred, because the power output differs too much to assume linear scaling. Therefore, the configuration is divided into subcomponents and their masses are estimated individually.

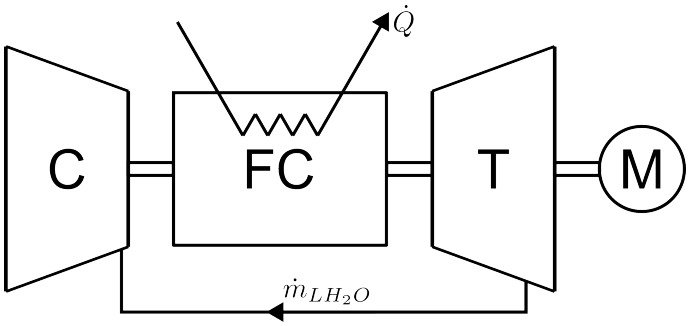

Figure 3.11: System for high altitude fuel cell operation

Figure 3.11 shows the most feasible configuration designed in [102] for operation at 18 km altitude. It consists of a compressor that pressurizes the outside air to 1.41 bar, followed by an evaporator that moisturizes and cools the air. This air can then be used by the fuel cell. A small portion of the waste heat generated by the fuel cell is transferred to the reaction air, as is the water vapour produced by the reaction. After that, the pressurized air is relaxed in a turbine, recapturing some of the work done by the compressor. During the relaxation process, the water condenses, releasing a lot of latent heat which is significant for the work done by the turbine. The condensed water is then recaptured through a separator and recycled into the evaporator. An electric motor is attached to the compressor shaft, filling the gap between the work done by the compressor and turbine, while doubling as a starter.
For the mass estimates, the mass of the fuel cell and its subsystems and the mass of the air conditioning system were estimated separately.
When talking about the gravimetric energy density of the fuel cell, not only the stack but also secondary systems are included. Predicting this gravimetric energy is difficult since there are currently multiple stack technologies being developed concurrently. Furthermore, the automotive industry is one of the driving forces behind the research and is likely to be the dominant industry in terms of production volumes; its chosen technology will benefit the most from the economics of scale [89]. Therefore, a non-optimal technology in terms of gravimetric energy density might be chosen for its lower cost and better reliability. Predictions for the gravimetric power density until 2040 range between 2 kW/kg and 3 kW/kg for the entire system, including cooling. Predicted efficiencies between 60 % and 70 % can be found [29], [30]. Since it is planned to operate the fuel cell at maximum efficiency during loitering and the gravimetric power density is calculated regarding the maximum power output, regardless of efficiency, it is assumed that for a system operating at maximum efficiency, a gravimetric power density of 1 kW/kg is reached. To account for further adaptations of the system to the outlined use case, namely modifications to the cooling system and water management system, as well as fuel supply and coolant lines, the total gravimetric power density is further reduced to 0.666 kW/kg. This assumes that these modifications have a mass fraction of 1/3. When this value is compared to currently available small-scale fuel cells, the predictions made would require an increase in gravimetric energy density of 33.3 %, which is deemed reasonable until 2040 [3]. Combining these conservative assumptions with current progress in research focused on expanding the operating environments of fuel cells [19], it can be assumed that a system delivering the performance required for our design can be realized by 2040.
To achieve the high pressure ratio required to supply the fuel cell with air at altitude, it is specified that the compressor will be a two-stage radial compressor, each stage with a pressure ratio of 4.2. While only using one stage, the small jet engines sold by JetCat feature pressure ratios and volume flows that are in the same order as expected for our system [42], therefore these will be the basis for the mass estimation of the air conditioning system When the performances and dimensions of these engines were analysed, it was found that they featured an average dimensionless mass-flow parameter of about

$$\frac{\dot{m} \cdot \sqrt{R \cdot T_t}}{A \cdot p_t} = 0.45 \tag{3.4}$$

This parameter was assumed to be the same for PERSEUS design, therefore the inlet area can be calculated. Furthermore, a clear correlation between the inlet area and the outer dimensions was found and used to model the size of an enveloping cylinder. To obtain an estimation of the mass, the effective density of those jet turbines was calculated and assumed to be constant. To achieve the pressure ratio a two-stage compressor is needed, therefore a basic assumption was made, that the second stage would increase the total length by 1/3 and double the radius of the enveloping cylinder. Although radial compressors tend to build on large radii, this assumption is very conservative and since a density is used to approximate the mass, the resulting mass estimation is conservative as well.
A quick parameter study for different power outputs of the system showed that a good approximation for the preliminary sizing process is to assume a total gravimetric energy density of 333.3 W/kg.
For the cooling system, the required cooling power is important and for an estimate the data obtained by [102] for the chosen configuration is used. This results in 0.57 kW of waste heat to be removed by the cooling system for every 1 kW of power generated.
To calculate the fuel consumption, an overall efficiency of the system of 50 % when operating at peak efficiency is assumed. While the stack itself will have an efficiency of 60-70 %, some of that power will be required for the motor that drives the compressor shaft.
The potential power output of this system will vary with altitude and is very difficult to predict as many factors can limit the power output, such as the stack itself, the cooling system, the fuel system and the air supply system. Therefore, only basic and conservative assumptions are made. One being that during the

VTOL phases, the fuel cell can supply twice the power supplied during loitering, albeit it is not operating at peak efficiency. Furthermore, to calculate the climb performance it is assumed, that the fuel cell will constantly supply the power it produces while loitering at altitude and is operating at peak efficiency. When analysing how the performance of other power plants differs with altitude, it becomes obvious that these assumptions are very conservative.
With all the calculations made above, the mass of the entire system can be calculated as a function of the power required during loitering, which is assumed to be the sum of the power required by the propulsion system, the payload and an additional 1 kW for secondary systems. For the final design, the preliminary sizing resulted in a power output of 12.24 kW at peak efficiency, with a system mass of 36.72 kg. Now a more accurate sizing could be done as mentioned above, resulting in a final mass of 34.88 kg and an encapsulating cylinder with a diameter of 22 cm and a length of 44 cm.
As mentioned in the battery section, fuel cells have a slow response to changes in power demand. If the current increases, at first the voltage drops, followed by a slow recovery [77]. This is where the battery system remains useful during normal flight, as it can compensate for these gaps in power output.
While some vapour in the exhaust is condensed in the turbine, removing all moisture in the exhaust through further condensation systems like e.g. a heat exchange is not feasible for the design. Therefore, the emitted moisture will increase the likelihood of the formation of contrails affecting the climate impact of the aircraft. However, this mechanism is not fully understood and is still being researched and since the exhaust does not contain soot, the formation mechanism of contrails differs from that of classical engine contrails [7].

3.7.3 Hydrogen Tank

Hydrogen offers the best gravimetric energy density of any fuel, but because of its low density, the resulting volumetric energy density is very low. To solve this, it can either be stored gaseous at high pressure or at very low temperatures as liquid hydrogen. Both approaches have their own set of challenges to overcome. But overall, both require a heavy tank, reducing the effective gravimetric energy to increase the volumetric energy density.
The Mass fraction

$$\mu_{Tank} = \frac{m_{LH_2O}}{m_{Tank}} \tag{3.5}$$

is a commonly used indicator to describe the gravimetric effectiveness of a storage system. Liquid storage systems achieve the highest mass fractions. A system with a mass fraction of $\mu_{Tank} = 33.3$ % has been realized in the internal hydrogen tank of the space shuttle, with a total hydrogen mass of 33 kg [69]. Furthermore, the FutPrint50 project predicts a fuel fraction between 30 % and 35 % [30]. Therefore, for future consideration, a fuel fraction of 33.3 % is assumed.
Gaseous storage systems offer a greater degree of freedom in the design process, as the storage pressure can be varied to tune the volumetric and gravimetric energy density. Since a higher tank pressure and therefore volumetric energy density will require a heavier tank and therefore diminish the gravimetric energy density [69]. High-pressure tanks working at 700 bar are currently commercially available, with 1000 bar tanks being in the works [81]. Because of the long mission duration and therefore large amount of hydrogen needed, high-pressure systems are not viable since the effective gravimetric energy density they offer is too small. Low-pressure systems have size problems, so it was considered to integrate low-pressure tanks into the wings of the aircraft. They would double as load-bearing components, saving mass, as beams could be omitted. Still, this approach ran into size problems, as the mission duration requires too much hydrogen to be stored. However, for future aircraft with shorter mission durations, this design was deemed very promising. Another disadvantage of this design is the expected high manufacturing cost of the wing due to its complex internal shape. Furthermore, as the wings are a relatively high-risk area for impact damage, this design might run into issues with repairability.
Because of the reasons mentioned above, a liquid hydrogen storage system was chosen. With the predicted mass fraction and the gravimetric density of hydrogen, an effective gravimetric density of 8.33 kWh/kg is achieved. As mentioned before, the expected overall efficiency of the fuel cell is 50 %. Therefore, the hydrogen storage system is sized to provide the energy needed during loitering for the targeted duration of 20 hours at a resulting gravimetric density of 4.1 kWh/kg. For the final configuration, the total mass of the liquid hydrogen and its tank was calculated to be 59.71 kg. The required internal volume was calculated using the density of liquid hydrogen and an insulation thickness of 10 cm was assumed.
Since liquid hydrogen is stored at a temperature that is always below ambient, it will heat up to its boiling point of -252 $°C$ and any further heat leaking in the air will result in hydrogen boiling off. This will increase the pressure inside the tank, therefore gaseous hydrogen must be vented. Since the fuel cell

needs gaseous hydrogen, it is optimal if the evaporation rate matches the consumption rate of the cell. If the hydrogen boils off faster, the excess must be vented into the environment and is lost. Consequently, it is optimal to tune the insulation of the system, so that the evaporation rate matches the average consumption rate of the fuel cell. Since the dominating flight phase is loitering at altitude and the power demand is very constant, the insulation will be tuned to match the consumption of the fuel cell at these conditions. As mentioned before, the fuel cell requires gaseous hydrogen, therefore a system is needed to increase the boil-off of hydrogen in case the fuel cell must provide more power, like it is the case during VTOL. A configuration capable of achieving this is described in [53], which simply adds a heater inside the tank. The power required for the heater cannot be used by the aircraft and there is a delay between the heater being switched on and the boil-off rate increasing. However, as the battery system is capable of handling sudden changes in power demand, this can be neglected in our chosen design.

3.8 Thermal Management

Maintaining optimal operating temperatures for all components ensures optimal system performance and assures reliability. A thorough study was conducted under the management of the University of Stuttgart to design and optimise thermal management and is the basis for PERSEUS' thermal management system [30].

Heat Source	Heat Sink
Batteries (VTOL)	Batteries (at loitering altitude)
Payload	Control Surfaces ice protection
Supercapacitor	Wing ice protection
Fuel Cell	Propeller ice protection

Table 3.2: Heat source and sink [1]

Table 3.2 shows all systems that produce heat and those that require heating. To minimise the amount of additional energy required for heating, it is beneficial to use the waste heat from cooling heat-producing components to supply other components.
With these requirements in mind, multiple management systems were analysed, such as using liquid coolant loops or heat conduction piping [1]. However, due to the added mass and complexity of these systems, they were omitted in favour of an open management system using air for heat transfer. As both heating and cooling are required, the system is based on two air ducts, one for hot air and one for cold air.
The thermal management air is provided by a NACA duct located at the front of the UAV, where a fan is installed to provide the required airflow both when stationary on the ground and when flying at altitude. The other NACA duct supplies reaction air to the fuel cell. Part of the air is used to cool the fuel cell and is then used as heating air, while the rest is used for cooling. All components are equipped with RTD sensors [96] and a management unit that controls the valves to provide an adequate flow of cooling and heating air to the components. All cooling and heating air is exhausted at the rear of the UAV as illustrated in figure 3.12.

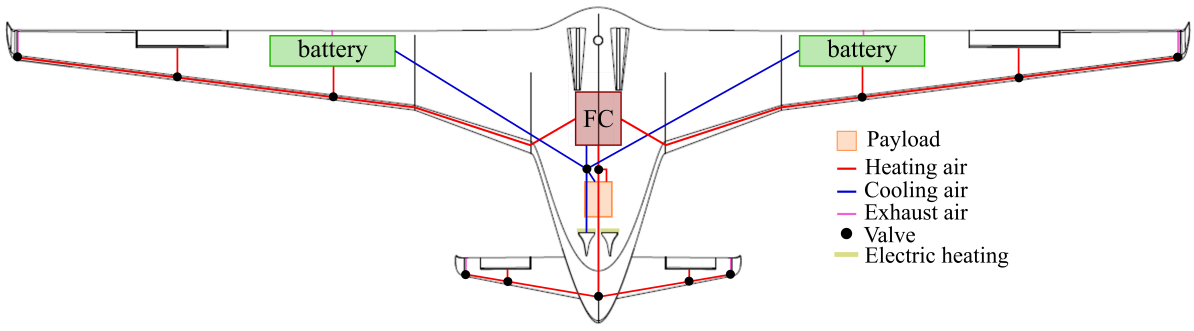

Figure 3.12: Thermal Flow of PERSEUS

A preliminary estimation for the needed inlet area was performed based on [62], resulting in a required area of 0.022 m^2. The inlet lips of the NACA ducts are electrically heated, as described in chapter 3.5.

3.9 Flight Control

In the following, positioning of the UAV during flight and landing is discussed in 3.9.1. Communication between UAV and MGS, other cooperative and non-cooperative aircraft and within the fleet is explained in 3.9.2 and navigation is further explained in 3.9.4. An overview of PERSEUS' systems is given in 3.9.5 and their integration is discussed in 3.9.6. The chapter is completed by a consideration of cybersecurity 3.9.7.3.13 gives an overview of the flight control and communication components.

3.9.1 Localization

Mid-air positioning The UAV is equipped with different sensors commonly used in aviation to determine position and flight attitude. An Inertial Measurement Unit (IMU), containing accelerometers, angular rate sensors and magnetometers, is installed in a low-vibration environment far from current-carrying components to ensure accurate measurements. Angle of Attack (AoA) sensors measure the oncoming flow. For altitude, air speed and vertical speed, a pitot tube is installed.
To determine their global position, aircraft normally use GNSS data as well as radio frequency (RF) signals from ground based VHF omnidirectional range/distance measurement equipment (VOR/DME) stations [28]. Since PERSEUS is mainly developed as a first-aid post-catastrophe system, we must act on the assumption that ground based RF sources are destroyed and no longer usable. It is also important not to rely solely on satellite-based GNSS in order to be independent of other countries and private companies. PERSEUS is equipped with a GNSS antenna and receiver, but a backup system is needed in case that GNSS data is not available.
If the GNSS signal is lost for only a short amount of time, the UAV can estimate its position out of the last received GNSS signal or the mission starting point at the ground station out of IMU data. However, this data is subject to drift, which is normally compensated for by GNSS data, so it is not a reliable solution for long-term state estimation.
State estimation can be realized by several methods. Additional to the conventional GNSS systems, vision-based and active ranging sensor solutions exist [46]. The problem of camera systems is their weather dependence. PERSEUS must be ready for use in any weather condition, therefore camera-based state estimation is not applicable. Active ranging sensors include LiDAR, radar, sonar and active infrared sensors. State-of-the-art applicable radar systems capable of covering the 18 km range between the UAV and the ground are too heavy for PERSEUS, e.g. Echodyne's EchoShield radar weighing 17.8 kg [24]. Infrared sensors are also highly weather dependent and the range of commercial LiDAR and Ultrasonic sensors is too small to reach the ground's surface (e.g. RIEGL VZ-4000 with a range of 5600 m [36]). All these technologies using the earth surface as a reference seem not to be applicable for PERSEUS. Additionally, orientating on the ground is difficult because landmarks might be destroyed by the catastrophe.
This is why the system uses the other UAVs of the swarm to position them to one another. Weather dependent systems are applicable on cruising altitude since it is located above the weather pattern, but since localization should be possible during climbing and sinking, these methods are discarded. Also, the range between the UAVs is higher than the range between UAV and ground, which rules out the active ranging sensors. The idea is to use RF signals like normal aircraft systems, but not to depend on ground-based radio stations. So, the other UAVs emitting RF are used as references. This allows combining state estimation and communication within the swarm in one system. Communication will be further discussed in UAV-to-UAV. RF navigation can be realized by different techniques: Received Signal Strength (RSS), Angle of Arrival (AOA), Time of Arrival (TOA) or Time Difference of Arrival (TDOA) [43]. In TOA [95] and TDOA [73] approaches, time synchronization between the UAVs is necessary, which requires additional efforts. In AOA localization, position is determined by triangulation of the angle measurements collected by multiple UAVs [103]. In RSS localization, the strength of the received RF signal is used to determine the distance between the transmitting and receiving object [85].
PERSEUS uses both AOA and RSS methods to determine the distance and position of the individual UAV within the swarm. These techniques are also applied to the communication signal between the UAV and the Mobile Ground Station (MGS). Each UAV is capable to determine its position relative to the MGS and to the swarm. Since every UAV identifies these positions, they are compared and evaluated between the UAVs for better localization results.

Positioning during landing approach PERSEUS is equipped with different landing aid systems. For scheduled landings on the base station's landing pad, Real Time Kinematic (RTK) GNSS is used. Based on its known position, the MGS continuously transmits corrections of satellite GNSS signals. These corrections are received by the UAV, so it can compute its own precise position relative to the MGS [99]. RTK GNSS provides high accuracy for precision landings and has already been proved on moving ship platforms, which is also a possible use case for PERSEUS [45]. Since this technology relies on satellite data, the MGS is also equipped with a camera to be able to track the approaching UAV. The UAVs are equipped with a green flashing light from top to bottom of the front fuselage. This is required for drones flying at night [21]. To improve camera tracking and therefore landing at night, a red light is mounted on the fuselages rear side to be able to determine the UAVs position in space.
For emergency landings, none of these systems is available. This is why the UAV itself is equipped with a camera facing towards the ground. Using Computer Vision, the UAV is able to find a feasible landing location and estimate time and distance until touchdown. UAVs equipped with the radar black box provided by the DLR can improve this estimation by additional data.

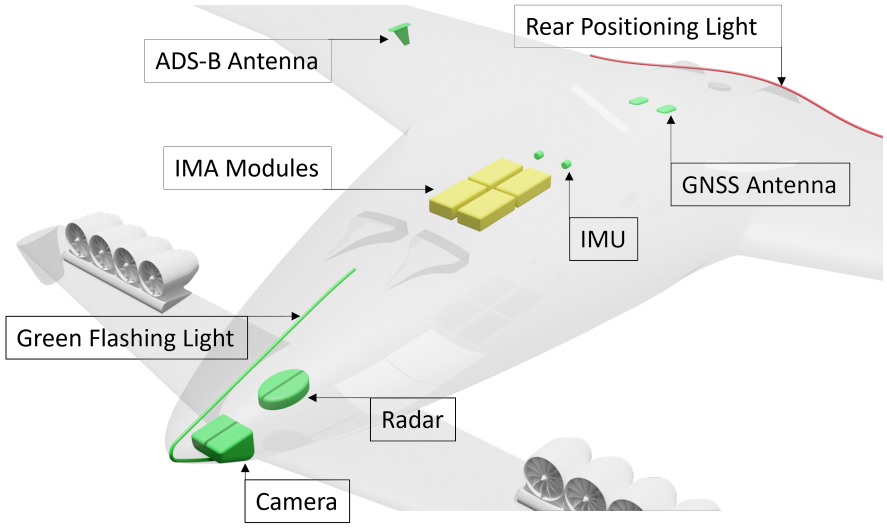

Figure 3.13: Overview of the flight control and communication components

3.9.2 Communication

UAV-to-MGS PERSEUS is a fully automatic system, only supervised by a small crew of pilots each monitoring multiple aircraft. It is not necessary to actively fly the UAV, but there is the possibility to interrupt in case of emergency or change of plans [88]. The communication between the UAV and the MGS is realized by C2 (command and control) links which address the line-of-sight spectrum [47], [63]. Both, MGS and UAV, are able to transmit and receive information, either in data or video form. It is also possible to transmit air traffic control communications over C2 links [47]. Broadcasting and reception at UAV side is realized by the rod antenna pre-specified by DLR.

UAV-to-UAV In the automotive industry and closely flying low altitude UAV swarms, Vehicle-to-Vehicle (V2V) links are used for communication [25], [80]. However, the range of WLAN or 4G/5G based V2V links is too short for the PERSEUS UAV-to-UAV communication. In inter-satellite communications, laser beams are used to transmit data. Lasers have high bandwidth, no electromagnetic interference and no licences are required to use the optical spectrum for communication. They have a very narrow beam size, so orientation must be highly precise to hit the target to communicate with. Also, the optical beam is degraded due to atmospheric effects [55]. Since atmospheric influence is relatively low in the stratosphere, free-space optical (FSO) communication is also possible for High Altitude Platforms (HAPs) [48]. To overcome the disadvantages of FSO communication, hybrid RF/FSO systems are being discussed that combine reliability in adverse weather conditions with the advantages of FSO [79], [50]. Even if this is a feasible solution to communicate in all operating altitudes of PERSEUS, a combined system of laser and RF communication is quite cost-intensive. This is why PERSEUS only communicates via RF signals, which are used for both communication and orientation. As a redundant system, there is also the possibility to communicate between two UAVs via the MGS.

UAV-to-cooperative aircraft To locate cooperative aircraft, the UAV disposes over an ADS-B transponder (in and out). With ADS-B, aircraft can communicate with air traffic control (ATC) and other ADS-B equipped aircraft to exchange information such as identification, position, altitude, speed and intention [64]. ATC commands avoidance manoeuvres which are considered within the Detect and Avoid System.

UAV-to-non cooperative aircraft Non-cooperative aircraft and other obstacles can't be detected by ADS-B. To ensure detection of all obstacles, non-cooperative sensors, such as lasers, radars, or cameras are needed [54]. A comparison of the different sensors is found in 3.3. Since PERSEUS is developed for missions in disaster areas, it must be able to function in all weather conditions. Radar systems are not weather dependent or sensitive to light and since the range of the system doesn't have to be as far as the range for localization determination, smaller and lighter systems can be used (e.g. Echodyne Echoflight with an instrumented range of 6 km and a mass of 0.73 kg [23]). This is why PERSEUS possesses over an additional radar system to detect non-cooperative aircraft.

Criteria	LiDAR	Radar	Ultra-sonic	Thermal and IR	Camera
Accuracy	High	High	Medium	Medium	Medium
Weather dependency	Low	No	Partial	High	High
Light sensitivity	No	No	No	No	Yes
Range	Medium	Long	Short	Medium	Short
Sensor size	Small	Large	Small	Small	Small
Processing requirement	Low	Low	Low	High	High
Power required	Medium	High	Medium	Low	Low

Table 3.3: Sensor attribute comparison for obstacle detection [104]

3.9.3 Detect and Avoid System

The detect and avoid system (DAA) consists of a collision avoidance (CA) system and a Remain-Well-Clear function (RWC).

Collision Avoidance The location of other aircraft and obstacles is determined by a surveillance and tracking module (STM). Inputs are the information from the ADS-B transponder and the radar modules. The STM conducts quality data checks and combines the inputs to an estimation of their position [67]. Considering the own position of the UAV as well as the information calculated by the STM, a threat resolution module (TRM) determines whether the intruder aircraft effects the route of the UAV. If so, a collision avoidance manoeuvre is calculated and initiated [67].

Remain-Well-Clear To predict risk of collision over a long period of time, the UAV communicates with air-traffic control (ATC) via ADS-B. If ATC and CA orders differ, CA instructions are the final layer to prevent mid-air collisions.

3.9.4 Navigation

Navigation is based on pre-programmed information, the DAA system, commands from the Ground Control Station and information provided by the other UAVs of the swarm. Before flight, routing information is loaded into the onboard autopilot system [63]. Further, inputs of the different communication systems (UAV-to-UAV, UAV-to-MGS, UAV-to-cooperative aircraft and UAV-to-non cooperative aircraft) are considered. To manage the different inputs and determine the resulting route, Artificial Intelligence (AI) is used.

3.9.5 System overview

Additional to the autopilot, the flight control system and the Detect and Avoid system, the UAV needs several other systems to retain safe flight. To avoid overheating or undercooling of important components such as fuel cell, batteries, engine and avionics, a thermal management system is installed. Fuel cell operation and the electric motors driving the EDFs must be regulated. A battery and supercapacitor

management system controls power supply, charging and discharge distribution.A battery and supercapacitor management system controls power supply, charging and discharge distribution. Also, landing gear and lights must be controlled.

3.9.6 Integrated Modular Avionics

The different systems are integrated with the integrated modular avionics (IMA) principle. To reduce mass, wiring, maintenance and future system update costs, the system functions are realized in one processing unit instead of several processors [31]. To avoid any interference between the different avionic tasks, they are separated in space and time. Each task is allocated memory and an execution window [5]. For redundancy of these flight essential functions, four IMA boxes are installed in each UAV.

3.9.7 Cybersecurity

In [6], cybersecurity vulnerabilities for UAVs are analysed, with the result that the main attack areas are navigation and communication. PERSEUS' high connectivity also leads to a larger attack surface. Cybersecurity is a complex area. A solution for the protection against cyber-attacks might be the implementation of a Host-based Intrusion Detection System (HIDS) which monitors the behaviour of an application and detects deviations from a legitimate model [32].

3.10 Performance

With all the calculations made in the previous sections, the final performance of the aircraft can be calculated and it can be verified that the target criteria are met.

Structure	63.2
Propulsion	37.5
Fuel cell system	34.9
Hydrogen and tank	59.71
Batteries	13
Payload	max. 13
Ailerons	10
Flight and power control	7
Wires and piping	7
Maximum Take-off Mass (MTOM)	**245.3 kg**

Table 3.4: Mass of system and subsystems [kg]

Table 3.4 shows the final mass estimation for the entire system and its subcomponents in the heaviest configuration. As mentioned in section 3.4, the current CAD model of the aircraft outperforms the preliminary predictions in terms of aerodynamics. However, since this model is neither fully optimized nor are all sources of drag considered, the L/D obtained from preliminary sizing will be used as a conservative estimation. A more precise calculation could be performed if the aerodynamic polars of the aircraft were known. Furthermore, it was noted in section 3.7 that it is very difficult to estimate the dependence of the power output of the powertrain on the altitude. Therefore, it is assumed that throughout the entire climb, the power output is equal to the power needed when loitering at altitude. Since the payload is only switched on when reaching the target, this additional power can be used by the propulsion system. Again, this assumption is very conservative.

VTOL Power	110 kW	L/D_{loiter}	24.77
Climb duration	2 h	Loitering power	12.24 kW
Climb distance	375 km	Return duration	1 h
Average climb rate	2.5 m/s	LH_2 for mission	15 kg
Loitering altitude	18 km	Sprint to scenario 2	1h 4 min
Loitering duration	17 h	Max. headwind for <2h	136.6 km/h
Loitering speed	294 km/h	Initial loitering at scenario 2	13h
$C_{L_{loiter}}$	0.47	Return from scenario 2	1h 4 min

Table 3.5: Performance during operation

Table 3.5 shows the relevant performances of the system for the two scenarios. The rate of climb decreases with altitude, but only the average climb rate from sea level to 18 km is shown. Since the battery system is capable of significantly increasing the power supplied to the propulsion system, a very high rate of climb can be achieved at any altitude, even if only for a short time. To calculate the loitering time at the target, it was assumed that half the energy required for the flight to the target was required for the return flight. When returning, the energy stored in altitude can be used to sustain flight and power is used only to support the avionics, therefore almost no fuel is used. However, the assumption made above considers the fuel reserves that must be maintained for unforeseen events while returning. In terms of mission, scenario 2 only differs from scenario 1 for the first UAV that arrives. For its replacements it has the same parameters as scenario 1 except its location. Because of the high average headwind allowed to still reach the target below 2 h, this requirement can be met at all conditions. All performance calculations are based on standard flight mechanics according to [72]. For alternative applications where the operation altitude is lower, the maximum loitering duration at altitude increases linearly to 38 h at 2 km altitude, assuming the same payload mass and power consumption. However, since the loitering speed decreases, the flight to target might take a substantial amount of time depending on the distance.

No.	Requirement	Achieved
1	Fly 100NM from base station to site of operation	X
2	Restore internet in Hamburg and Schleswig-Holstein	X
3	Return to base station and land	X
4	Travel 170 NM in less than 2h	X
5	Provide internet and location observation for 700km^2	X
6	Cover scenario 1 and 2 permanently	X
7	Fleet deployable up until 55th parallel	X
8	Entry into service in 2040	X

Table 3.6: Requirements

Table 3.6 shows the requirements that were made in section 2.1 and that they were all met. This can be confirmed with the calculations made in this chapter for all requirements except 5, 6 and 7. The reasons why these are also met are given in the following sections.

4 Operation

4.1 Mission Scenarios

The two emergency scenarios, which have been specified in the task definition, can be completely solved by the PERSEUS system. In the first scenario, the two areas to be monitored have different coverage requirements. While Schleswig-Holstein is very large in terms of area, the defining factor for the city of Hamburg is its population density. For both cases, a self-developed algorithm was used to determine the optimal area coverage by means of circles representing the Internet coverage. This is achieved by placing a grid onto the polygon shaped outlines, which is then completely covered using circles. In addition, another algorithm is used to detect and minimize overlaps. The area coverage of Schleswig-Holstein is shown in figure 4.1.
To achieve complete coverage, a total of 33 UAVs for the mainland and one UAV for the island of Heligoland is necessary. The 33 UAVs follow a certain flight-path, that is pre-programmed into the board computer. The single UAV circles above the island.
For Hamburg, the area coverage is shown in figure 4.2. Only three UAVs are necessary to cover the entire city area. However, due to the high population density, seven internet relays meaning seven UAVs are needed to achieve an internet speed of 0,1 Mbit/s per capita. Due to the modular payload design, a UAV can be equipped with two internet relays instead of one relay and a radar. Therefore, only four UAVs are necessary to provide sufficient Internet speed for the entire city. Three UAVs are equipped with two Internet relays and one with a relay as well as a radar to be able to react in case scenario 2 occurs. Another UAV is used to cover the island of Neuwerk, which only has a single Internet relay as payload, therefore being slightly lighter and enabling a longer cruise time.

For scenario 2, it is defined in the task description that a UAV is within 170 nautical miles of the emergency area with a size of 700 km^2. This area must be reached within 2 hours and covered completely

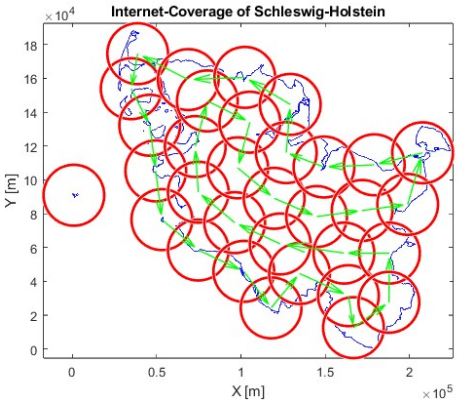

Figure 4.1: Internet-Coverage of Schleswig-Holstein

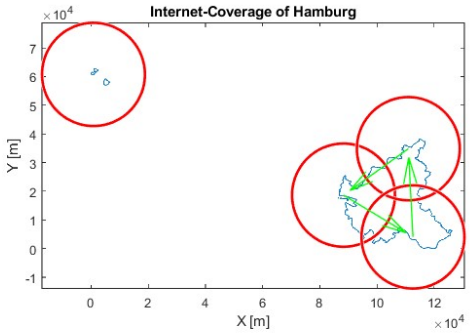

Figure 4.2: Internet-Coverage of Hamburg

via a radar. Since the UAV is flying at 18 kilometres altitude, the radar circle projected onto the ground has an area of 1017.87 km^2. Therefore, only one UAV is necessary to cover the entire area. As soon as emergency scenario 2 occurs, the UAV equipped with the radar module starts sprinting to the target destination. Meanwhile, another UAV launches from the base of operations to fill the gap in Internet coverage that has been created.

4.2 Alternative Use-Cases

There are numerous alternative Use-Cases for the UAV fleet, since the payload is easily changeable. An overview of some possible scenarios is shown in 4.3.

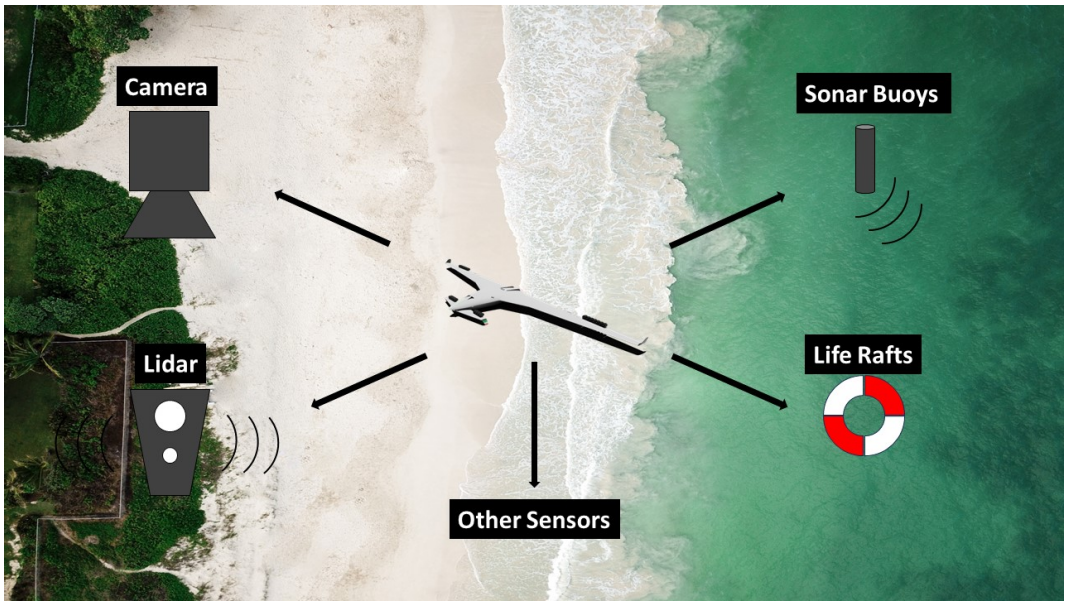

Figure 4.3: Alternative Use-Cases

Deployment scenarios exist both on water and land. Over water, sonar buoys that are dropped in the water can be used to locate missing boats. One UAV can carry at least 2 buoys. This allows a fleet to cover very large areas with sonar. A UAV can also carry a combination of a sonar buoy and a miniature life raft. If a ship has sunk and has been detected by sonar, a life raft can be dropped to provide immediate assistance to the shipwrecked. Due to the VTOL capability of the system, it is also possible to land on aircraft carriers or the helipad of ships and re-equip. In addition, Lidar sensors can be equipped for area mapping or research. Further, a camera system can be mounted for situation monitoring, e.g. at major sporting events to help monitor traffic or coordinate emergency services. These other payloads also impose a different optimum flight altitude, which will be below 18 km, allowing PERSEUS to achieve even

longer flight times. In addition, the high possible flight altitude opens up further research possibilities, such as stratospheric research or aerosol research.

4.3 Transportation and Deployment

Since the overall system will not only be used in the area of emergency scenarios, but a worldwide operational readiness is to be achieved and thus numerous scenarios are to be covered (see 4.2), two different deployment scenarios were devised.
To increase the mobility of the overall system, the first deployment scenario uses standard mega trailers [59]. These can be easily transported to the various target areas by trucks and use the already existing infrastructure. Each trailer is capable of transporting eight UAVs, which is why six trucks are needed for the emergency scenarios in order to have sufficient replacements. To increase usability, each truck is a standalone unit that serves as a mobile ground station for its fleet of UAVs.
Once at the target area, the trailer can be unfolded and converted into a landing platform using supports. The PERSEUS UAV, which are stored in a rack, can be pushed to the side using guides and then set up one after the other on the open space by a maximum of three workers. For a group of inexperienced workers, an assembly time of up to 40 minutes is expected, whereas experienced workers can fully assemble the UAV in under 20 minutes.
Only then is the UAV refuelled to ensure the required safety for the crew and, in parallel, carries out the necessary take-off checks. After that, the UAV can take off independently and fly to the target area with the four other UAVs assembled in parallel on the remaining trucks. Figure 4.4 visualizes this procedure. The sixth truck, which contains the spare PERSEUS UAVs, is used only as a backup landing platform and for repairs or maintenance and replacement of payload on site.

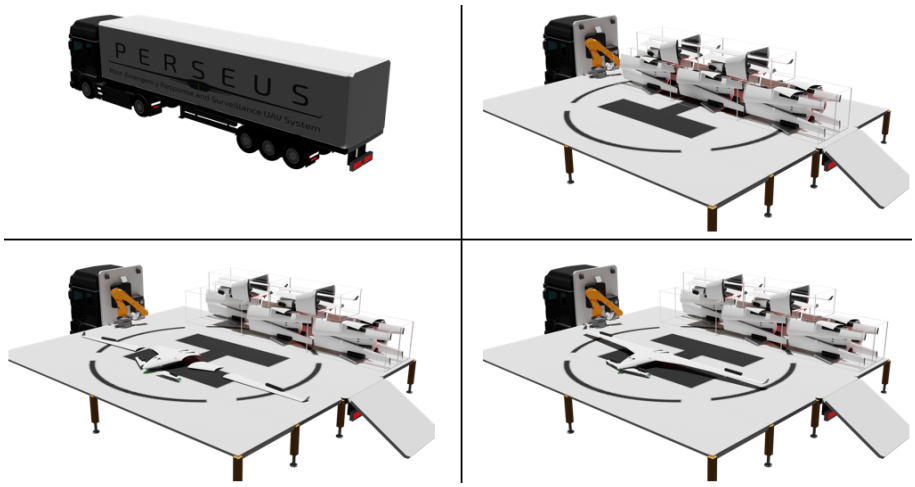

Figure 4.4: Deployment of the trailer and included UAVs

The second concept addresses scenarios that require rapid response readiness or where an occurrence can already be foreseen or the area to be covered is already known. Such scenarios include, for example, Canadian wildfires, which increasingly require support and demand some level of preparedness [15], [93], floods and hurricanes, for which warning systems are becoming increasingly accurate [84] and which cause more damage as coastal populations and infrastructure grow [75]. As a variation of the mobile scenario, the PERSEUS System can be brought to the target area in advance or can be waiting at an airfield already assembled for their deployment. This would reduce the deployment time by several hours, since both transport and assembly time are eliminated.

4.4 Ground Station

The worldwide distribution of airports and power plants is displayed in Fig. 4.5. It clearly shows that outside of Europe and America, the coverage is getting increasingly weaker. This means that PERSEUS should operate independently of both surface conditions and energy supply. The ground station must therefore provide the UAVs with a stable take-off and landing platform for refuelling and maintenance.

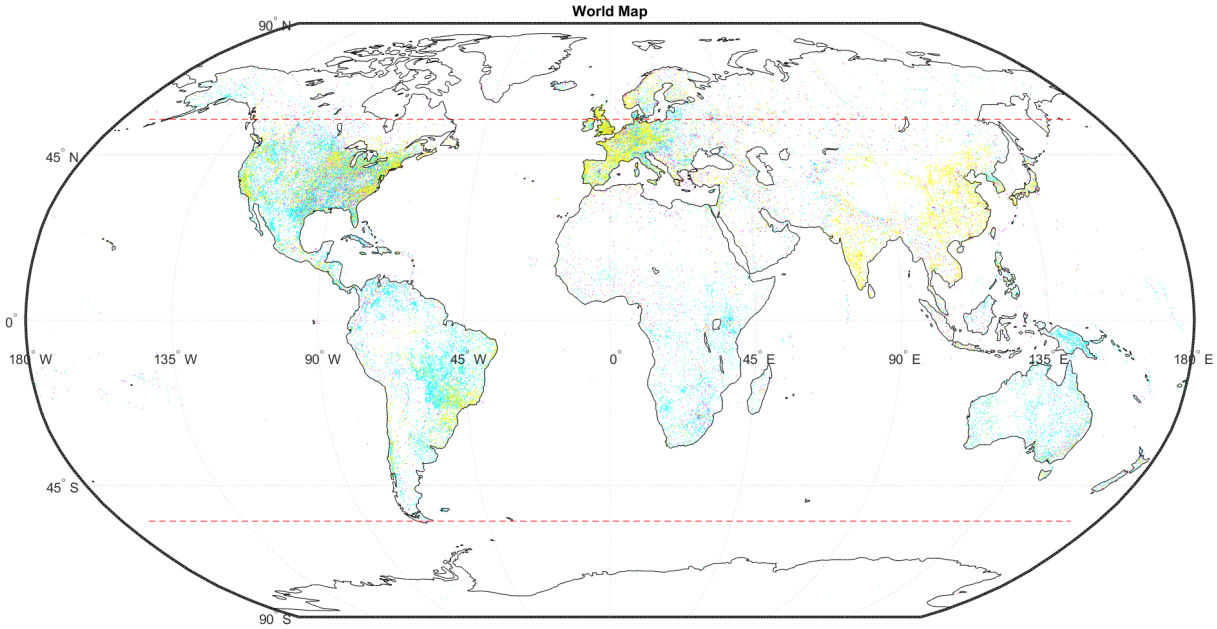

Figure 4.5: Power plants (yellow) [35], airports (blue) and navigational aids (magenta) worldwide [66]

4.4.1 Hydrogen Supply Chain

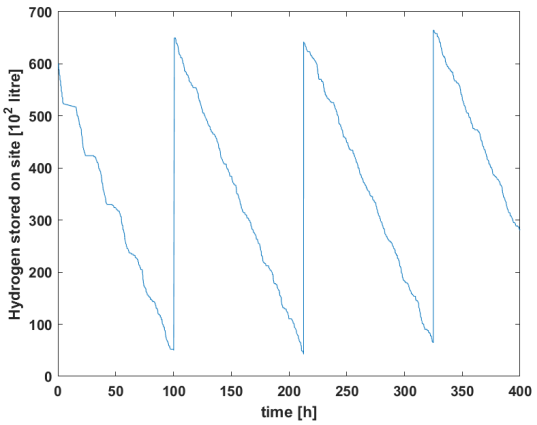

Figure 4.6: Hydrogen stored on site near the ground station

As the PERSEUS UAV uses liquid hydrogen, a steady supply is needed. Due to the growing interest in the hydrogen market as a sustainable energy source, an increasing number of production facilities and production methods are emerging. Worldwide, there are almost 2000 different projects [40] on this subject, even in the area of the emergency scenarios, in Hamburg, the production of hydrogen is advanced [37], as well as in Rostock-Laage [97]. It is therefore assumed that a permanent supply of hydrogen will not be a problem by 2040.
Hydrogen can be either produced at power plants to reduce the power waste during off-peak hours [58] or on site by using electrolysis at suitable locations with access to electricity and water. Such electrolysis plants are already available in mobile container sizes [96], [60], [38] and even mobile production of hydrogen from biogas is possible [11].
A truck size of 60,000 litres was assumed for the supply of liquid hydrogen, which was taken from various recent product catalogues [52], [86] and scientific papers [41]. The hydrogen supply truck is meant as a local storage facility, remaining near the ground station until empty.
Figure 4.6 shows a Simulation of the hydrogen stored on site. Here, the varying flight time of the individual UAVs is taken into account and it is shown that a replenishment is necessary approximately every 110 hours or 4.5 days.

4.4.2 Mobile Ground Station

As mentioned in 4.3 a mobile scenario was devised. This includes a number of trailers as well as a hydrogen supply truck.
The mobile ground station offers various features, which will be explained in the following.
Since complete autonomy during operation is to be ensured, a robotic arm for automatic refuelling was implemented. Such systems have already been researched [26], [49] and are currently being tested [76], [74]. The arm will also be used for assembly and maintenance by lifting parts or the entire UAV, thus reducing the necessary loads for humans. For this, however, a certain safety standard must be

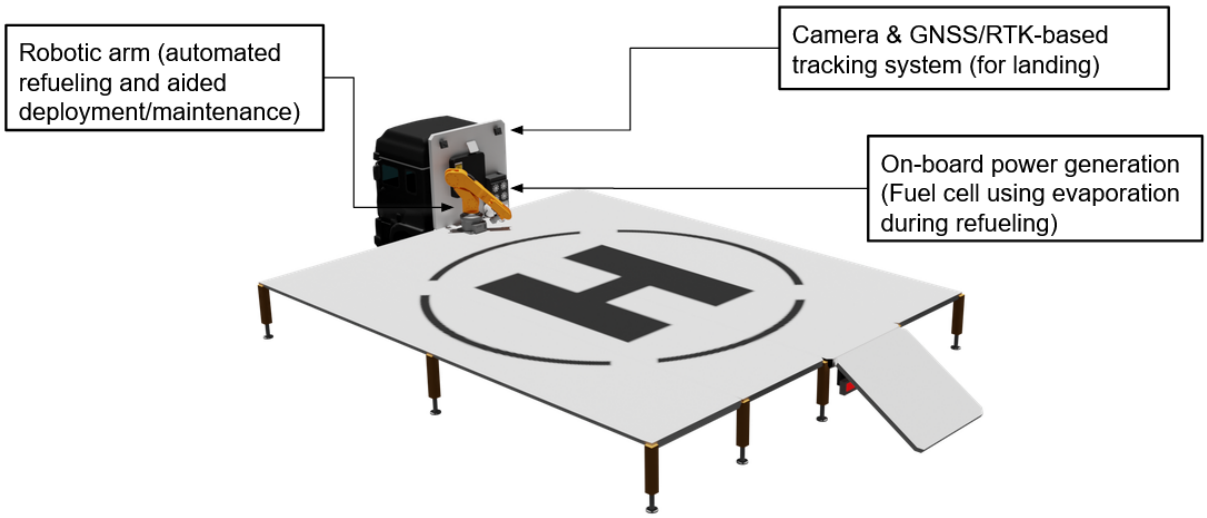

Figure 4.7: The mobile ground station

implemented on the robotic arm.
In order to reduce the loss due to evaporation of liquid hydrogen during the refuelling process, the possibility of purging and pre-cooling with liquid nitrogen [34] is proposed, which should bring the evaporation to below 5-9%. The duration of the tanking process including purging was assumed to be about ten minutes [56]. The station is to be supplied with power via its own onboard fuel cell. In addition, batteries will be installed for the power peaks. The system is thus similar to the hybrid power train (s. 3.7) installed in the UAVs, which is why no completely new development is necessary. The fuel cell receives its hydrogen in gaseous form from the boil-offs of the hydrogen supply truck and the vaporization during refuelling, both of which can be collected and stored until use. As mentioned in chapter 3.9.1, the ground station has a RTK GNSS system to support PERSEUS during landing. Furthermore, cameras were installed to track the position of the landing UAV, which is only possible in sufficient viewing conditions.
The ground station is equipped with an antenna and a processing unit for communication with the UAVs. This means that tasks requiring a lot of computing time, such as predictive maintenance or various flight path planing tasks, can be carried out by the ground station and only the finished data is sent to the fleet.

4.5 Maintenance

To minimize maintenance and storage costs and to improve safety, the principle of predictive maintenance is implemented. To realize predictive maintenance, the aircraft components are equipped with multiple sensors to monitor them during operation. The data is processed using statistics and machine learning to identify trends in component health. By constantly supervising the components, maintenance tasks can be scheduled according to their actual remaining life span and not in regular intervals like in case of preventive maintenance [100]. To process big sensor data, an additional processing unit is needed which takes up mass, space and energy. This is why sensor data will be sent to the ground station via C2 link where it is analysed.
As explained before, the time when maintenance is necessary can be precisely determined. However, it is unclear what the exact maintenance for new technology like the fuel cell system might look like. Although fuel cell systems have been heavily researched for years, little attention has been paid to the maintenance, repair and overhaul (MRO) aspect. In aviation, MRO has the purpose to ensure airworthiness and safe flight operations. Therefore, high safety and certification requirements are necessary, which are not represented in other industries. Nevertheless, some of the MRO experience gained in the automotive sector can also be applied to aviation. For instance, within the automotive industry, a similar notion is referred to as road-worthiness. While not as stringent in terms of regulations, it provides a first clue regarding possible regulations and certifications. Furthermore, the handling of hydrogen is a common feature of both sectors. The safe handling measures developed in the automotive sector can also be applied in aviation. Although the operating conditions in the two areas are not fully comparable, it is assumed that the failure modes are similar [39]. The most common failures for a PEM fuel cell are

flooding, drying, electrode poisoning or starvation [8]. Strategies to mitigate these effects are shown in figure 4.8.

Flooding	Drying
Decrease relative humidity of inlet gases	Increase relative humidity of inlet gases
Increase flow of inlet gases	Decrease flow of inlet gases
Increase stack temperature	Decrease stack temperature
Decrease current	Increase current
Poisoning	**Starvation**
Increase air flow	Increase air flow
Air bleeding	Increase hydrogen flow
	Increase pressure

Figure 4.8: Damage mitigation measures [39]

Knowing about these possible errors and how to avoid them correctly can therefore be of great value for the safe operation of PEM fuel cells in aviation. Together with predictive maintenance, a safe and cost-efficient maintenance concept can thus be developed until 2040.

5 Cost Estimation

Due to the relatively small amount of liquid hydrogen required per day for operation, the cost of hydrogen is increasing. However, [98] shows that with the help of glass fibre tube trailers, the cost of supplying hydrogen can be reduced by about one-third. In addition, the cost of producing hydrogen should be significantly reduced by 2040, due to increasing demand. A 2006 estimate shows that the cost will be reduced to less than \$1/kg by 2017 [68]. However, current costs (as of 2019), using California as a case study, are closer to \$5.38/kg for a complete supply chain [14]. Therefore, a value of \$3/kg is assumed.
Both the Life Cycle Costs [51] and the Direct Operating Costs (DOC) [92] were estimated using empirical formulas and benchmarks [87]. In order to have a better comparison, the Direct Operating Cost are therefore compared with those of other high altitude platforms in figure 5.2.

Life Cycle Cost [Mio. \$]		**Direct Operating Cost** [Thousand \$/a]	
Design/Engineering	67.73	Personal	1939
Tooling	8.61	Fuel	18.15
Production	11.62	Maintenance	3063
Quality Assurance	2.64	Landing	1.91
Bill of Material	8.95	Ground Handling	0.76
Propulsion (8%) [101]	10.62	Navigation	26.96
Avionic (17%) [101]	22.56	Capital	5211
Total	**132.73 [Mio.-\$]**	**Total**	**10.26 [Mio.-\$/a]**

Table 5.1: Total Cost of PERSEUS Fleet separated in Life Cycle and Direct Operating Cost

It should be noted, that these numbers use estimations based on General Aviation aircraft, therefore relying on combustion or jet engines and are not fully adequate for an electric UAV system. However, since no accurately comparable aircraft with official prices exist, these estimates provide a good initial baseline.
Furthermore, the number of total fleets should be taken into account, as the price for a single system decreases with the total number of UAVs produced and sold. This trend can be seen in figure 5.1, where the price is \$2.77M per UAV for a production number of exactly one fleet. With three fleets, the price already lowers to more than half and decreases further as the number of fleets increases.
Figure 5.2 shows the difference in DOC compared to three other drones. The individual parts of the total DOC have been estimated using [101].

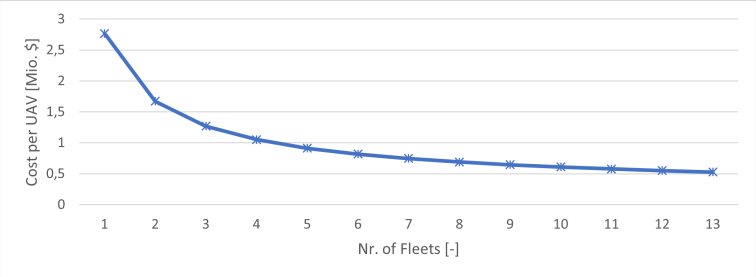

Figure 5.1: Cost per UAV with increasing production numbers

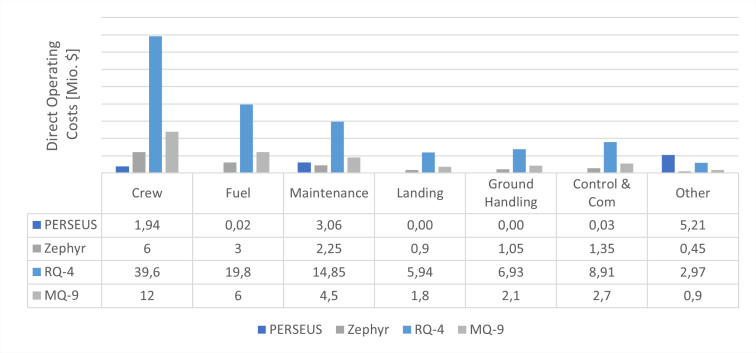

	Crew	Fuel	Maintenance	Landing	Ground Handling	Control & Com	Other
PERSEUS	1,94	0,02	3,06	0,00	0,00	0,03	5,21
Zephyr	6	3	2,25	0,9	1,05	1,35	0,45
RQ-4	39,6	19,8	14,85	5,94	6,93	8,91	2,97
MQ-9	12	6	4,5	1,8	2,1	2,7	0,9

Figure 5.2: DOC compared with other aircrafts

6 Future Applications and Perspective/ Conclusion

As climate change continues to advance, the number of extreme weather phenomena is steadily increasing [4]. As a result, communication and internet services are increasingly disrupted. Rapid restoration of communication and internet is essential to coordinate emergency services. The PERSEUS UAV system developed in the course of the DLR Design Challenge 2023 presents an innovative and sustainable concept that can solve the above problems reliably and quickly. Electric ducted fans are mounted on the ailerons of the wing as well as the canard, giving PERSEUS VTOL capabilities, which ensures independence from airfields with the mobile ground station increasing mobility and complete autarky from the mission location. A hybrid propulsion system consisting of hydrogen fuel cells, batteries and super capacitors provides the necessary energy and enables sustainable operation. In addition, the payload of the system can be easily exchanged, which opens up further areas of application. This makes PERSEUS a unique and innovative concept with highly competitive flight time and flexibility.

Looking ahead, new improvements in the energy density of batteries and fuel cells can further increase and improve the operational scope of PERSEUS in the future, ensuring the future-proofing of the design. In addition, the use of AI could help to develop improved operational concepts to further optimise the flight paths, thus minimizing the amount of UAVs needed.

A major factor of uncertainty that became apparent during the conceptual design process is the fuel cell, which still has to be fully operational and efficient at this extreme altitude. Research is currently underway and experts agree that this concept is even currently in the year 2023 feasible. This was also confirmed in an expert interview conducted with an engineer from H3 Dynamics [70]. However, it remains to be seen what level of technology this field of study will reach by the year 2040.

References

[1] "A review on the recent developments in thermal management systems for hybrid-electric aircraft". In: (2023).

[2] Institute of Aerodynamics and Gas Dynamics University of Stuttgart. "Aero 5.6". In: ().

[3] "AEROSTAK HYDROGEN FUEL CELL SYSTEMS FOR UAS". In: (2022).

[4] European Environment Agency. *Europe's changing climate hazards*. EEA report (Online). Publications Office, 2021. DOI: 10.2800/458052. URL: https://data.europa.eu/doi/10.2800/458052.

[5] Ahmad Al Sheikh et al. "Strictly periodic scheduling in IMA-based architectures". In: *Real-Time Systems* 48 (2012), pp. 359–386.

[6] Rui Carlos Josino Alexandre, Luiz Eduardo Galvão Martins, and Tony Gorschek. "Cybersecurity Risk Assessment for Medium-Risk Drones: A Systematic Literature Review". In: *IEEE Aerospace and Electronic Systems Magazine* (2023).

[7] *Analysing the contrails of the future*. DLR. https://www.dlr.de/en/latest/news/2022/03/20220720_analysing-the-contrails-of-the-future; 2022.

[8] Julie AUBRY et al. "Fault tolerant control of a Proton Exchange Membrane Fuel Cell based on a Modified Failure Mode and Effect Analysis". In: *2020 IEEE Vehicle Power and Propulsion Conference (VPPC)*. 2020, pp. 1–5. DOI: 10.1109/VPPC49601.2020.9330864.

[9] "Ausgewählte Lösungen zu Auftriebsanstieg und induziertem Widerstand". In: TU Dresden.

[10] *Aviation Word: Service ceiling*. Experimental Aircraft Association EAA. https://www.eaa.org/eaa/news-and-publications/eaa-news-and-aviation-news/bits-and-pieces-newsletter/09-13-2016-aviation-word-service-ceiling#:~:text=The%20definition%20of%20the%20service%20ceiling%20is%20the,aircraft%20begins%20to%20run%20out%20of%20climb%20capability.; 2016.

[11] *BtX energy: Schlüsselfertige Komplettlösung für regionalen Wasserstoff aus Biomasse*. Solarserver. https://www.solarserver.de/2021/01/19/btx-energy-schluesselfertige-komplettloesung-fuer-regionalen-wasserstoff-aus-biomasse/; 2021.

[12] *Centre for High Altitude Platform Applications*. University of York. https://www.york.ac.uk/chapa/; 2023.

[13] "Charging strategy effect on lithium polymer battery capacity: A case study". In: *INTERNATIONAL JOURNAL OF ENERGY AND ENVIRONMENT* (2020).

[14] Elizabeth Connelly et al. "Current status of hydrogen liquefaction costs". In: *DOE Hydrogen and Fuel Cells Program Record* 19001 (2019).

[15] Sean CP Coogan et al. "Scientists' warning on wildfire—a Canadian perspective". In: *Canadian Journal of Forest Research* 49.9 (2019), pp. 1015–1023.

[16] *COTEXX KNITTED HEATING FABRIC*. CoTexx. https://cotexx.de/en/heating-fabric-for-tools-and-deicing-composites/;

[17] Isaac M. Daniel. "Dynamic Failure of Materials and Structures". In: Springer, 2010. Chap. Impact Response and Damage Tolerance of Composite Sandwich Structures.

[18] Jan-Philipp Buch Dennis Vechtel. "Aspects of yaw control design of an aircraft with distributed electric propulsion". In: *CEAS Aeronautical Journal* (2022).

[19] "Designing the next generation of proton-exchange membrane fuel cells". In: (2021).

[20] Prof. Franz Joseph Arendts Dipl. Ing. Maged Sorour Prof. Dr. Ing. Peter Middendorf. "Leichtbau". In: (2012).

[21] *Drohnen*. Luftfahrt-Bundesamt. https://www.lba.de/DE/Drohnen/FAQ/01_FAQ_Allgemein/FAQ_node.html; accessed on 11.07.2023. 2023.

[22] EASA. "Powered by EASA eRules Page 2 of 100| Jun 2023 Easy Access Rules for Normal-Category Aeroplanes (CS-23) (CS Amendment 5, AMC/GM Issue 3)". In: (2023).

[23] Echodyne. "EchoFlight®Airborne DAA Radar". In: (2023).

[24] Echodyne. "EchoShield® Multi-Mission 4D Radar". In: (2023).

[25] Linus Chibuzo Ezenwa. "Drahtlose V2V-Kommunikation mit DSRC-Technik im Vergleich zu C-V2X". In: *ATZ-Automobiltechnische Zeitschrift* 124.6 (2022), pp. 42–45.

[26] Aly Farag et al. "Monocular, vision based, autonomous refueling system". In: *Sixth IEEE Workshop on Applications of Computer Vision, 2002.(WACV 2002). Proceedings.* IEEE. 2002, pp. 309–313.

[27] Cher Ming Tan Michael Pecht Feng Leng. "Effect of Temperature on the Aging rate of Li Ion Battery Operating above Room Temperature". In: *Scientific Reports* (2015).

[28] Walter Fichter and Johannes Stephan. *Flugregelung: Theoretische Grundlagen für die Lenkung und Regelung von Flächenflugzeugen.* Springer-Verlag, 2020.

[29] "FUEL CELLS Roadmap Report". In: (2022).

[30] "FutPrInt50, D3.1: Sub-system Enablers and Technology Gaps". In: (2020).

[31] Thomas Gaska, Chris Watkin, and Yu Chen. "Integrated modular avionics-past, present, and future". In: *IEEE Aerospace and Electronic Systems Magazine* 30.9 (2015), pp. 12–23.

[32] Marc Gatti and Aliénor Damien. "AI, connectivity and cyber-security in avionics". In: *2019 24th IEEE International Conference on Emerging Technologies and Factory Automation (ETFA).* IEEE. 2019, pp. 35–38.

[33] *GE-Ryan XV-5A.* The Vertical Flight Society. `https://vtol.org/vstol/VSTOLWheel/GE-RyanXV-5A.htm`; accessed on 10.07.2023.

[34] Fardin Ghaffari-Tabrizi, Jan Haemisch, and Daniela Lindner. "Reducing Hydrogen Boil-Off Losses during Fuelling by Pre-Cooling Cryogenic Tank". In: *Hydrogen* 3.2 (2022), pp. 255–269.

[35] *Global Power Plant Database.* World Resources Institute. `https://datasets.wri.org/dataset/globalpowerplantdatabase`; 2023.

[36] RIEGL Laser Measurement Systems GmbH. "RIEGL VQ®-840-GL". In: (2023).

[37] *Green hydrogen from Moorburg.* future hamburg. `https://future.hamburg/en/project-brief-elektrolyseur-green-hydrogen-moorburg`; 2021.

[38] *H-TEC PEM-Elektrolyseur ME450.* H-TEC Systems. `https://www.h-tec.com/produkte/detail/h-tec-pem-elektrolyseur-me450/me450/`; 2023.

[39] Tim Hoff et al. "Implementation of Fuel Cells in Aviation from a Maintenance, Repair and Overhaul Perspective". In: *Aerospace* 10.1 (2023). ISSN: 2226-4310. DOI: 10.3390/aerospace10010023. URL: `https://www.mdpi.com/2226-4310/10/1/23`.

[40] *Hydrogen Projects Database.* iea. `https://www.iea.org/data-and-statistics/data-product/hydrogen-projects-database`; 2022.

[41] Simon Jallais. "Pre-Normative Research for Safe use of Liquid HYdrogen (PRESLHY)". In: *Fuel Cells and Hydrogen Joint Undertaking* (2018).

[42] *JetCat.* `https://www.jetcat.de/de`;

[43] Xinhua Jiang et al. "Localization of multiple RF sources based on Bayesian compressive sensing using a limited number of UAVs with airborne RSS sensor". In: *IEEE Sensors Journal* 21.5 (2020), pp. 7067–7079.

[44] Jr John D. Anderson and Christopher P. Cadou. *Fundamentals of Aerodynamics, Seventh Edition.* McGraw Hill LLC, 2024.

[45] Youngshin Kang et al. "A precision landing test on motion platform and shipboard of a tilt-rotor UAV based on RTK-GNSS". In: *International Journal of Aeronautical and Space Sciences* 19 (2018), pp. 994–1005.

[46] Farid Kendoul. "Survey of advances in guidance, navigation, and control of unmanned rotorcraft systems". In: *Journal of Field Robotics* 29.2 (2012), pp. 315–378.

[47] Robert J Kerczewski, Jeffrey D Wilson, and William D Bishop. "Satellite Communications for Unmanned Aircraft C2 Links: C-Band, Ku-Band and Ka-Band". In: *AIAA International Communications Satellite Systems Conference.* GRC-E-DAA-TN35493. 2016.

[48] Yana Kremenetska et al. "High-Altitude Configuration of Non-Terrestrial Telecommunication Network using Optical Wireless Technologies". In: *International Journal of Communication Networks and Information Security* 13.3 (2021), pp. 394–400.

[49] Leahy, Shiu, and Andersen. "Robotic aircraft refueling: a concept demonstration". In: *IEEE 1991 International Conference on Systems Engineering*. IEEE. 1991, pp. 320–323.

[50] Ju-Hyung Lee et al. "Spectral-Efficient Network Design for High-Altitude Platform Station Networks With Mixed RF/FSO System". In: *IEEE Transactions on Wireless Communications* 21.9 (2022), pp. 7072–7087.

[51] Grant Carichner Leland M. Nicolai. *Fundamentals of Aircraft Design*. American Institute of Aeronautics Astronautics, 2010.

[52] *LH2 TRANSPORT TRAILERS*. Chart Industries. `https://files.chartindustries.com/21746492_LH2Trailer.pdf`; 2022.

[53] "Liquid hydrogen fuel system design and demonstration in a small long endurance air vehicle". In: (2017).

[54] Imen Mahjri, Amine Dhraief, and Abdelfettah Belghith. "A review on collision avoidance systems for unmanned aerial vehicles". In: *Communication Technologies for Vehicles: 8th International Workshop, Nets4Cars/Nets4Trains/Nets4Aircraft 2015, Sousse, Tunisia, May 6-8, 2015. Proceedings 8*. Springer. 2015, pp. 203–214.

[55] Arun K Majumdar. *Laser Communication with Constellation Satellites, UAVs, HAPs and Balloons*. Springer, 2022.

[56] Jonas Mangold et al. "Refueling of LH2 Aircraft—Assessment of Turnaround Procedures and Aircraft Design Implication". In: *Energies* 15.7 (2022), p. 2475.

[57] Johannes S. E. Soikkeli Maurice F. M. Hoogreef. "Flight dynamics and control assessment for differential thrust aircraft in engine inoperative conditions including aero-propulsive effects". In: *CEAS Aeronautical Journal* (2022).

[58] Kaveh Mazloomi and Chandima Gomes. "Hydrogen as an energy carrier: Prospects and challenges". In: *Renewable and Sustainable Energy Reviews* 16.5 (2012), pp. 3024–3033.

[59] *Mega Trailer*. DSV. `https://www.dsv.com/de-de/unsere-loesungen/transportarten/landtransport/anhaengergroessen/mega-trailer`. 2023.

[60] *Mobile Containerlösung zur Herstellung von Wasserstoff aus Windstrom*. Windkraft-Journal. `https://www.windkraft-journal.de/2018/12/31/mobile-containerloesung-zur-herstellung-von-wasserstoff-aus-windstrom/131287`; 2018.

[61] "Morphing Wing Technologies". In: MDPI, 2018.

[62] Emmet A. Mossman and Lauros M. Randall. "RESEARCH MEMORANDUM AN EXPERIMENTAL INVESTIGATION OF THE DESIGN VARIABLES FOR NACA SUBMERGED DUCT ENTRANCES". In: (1948).

[63] J Chris Naftel. "NASA Global Hawk: Project overview and future plans". In: *International Symposium on Remote Sensing of Environment*. DFRC-E-DAA-TN3204. 2011.

[64] Civil Aviation Authority of New Zealand. "ADS-B in New Zealand: Information for aircraft owners, operators, maintainers, and crew". Version 2. In: (2020).

[65] Hedda Nier. *So unterschiedlich lang sind die Tage in Deutschland*. Statista. `https://de.statista.com/infografik/17559/tageslichtdauer-in-deutschland/#:~:text=So%20ist%20der%20k%C3%BCrzeste%20Tag,mehr%20als%20eine%20Stunde%20l%C3%A4nger.`; 2019.

[66] *Open data*. OurAirports. `https://ourairports.com/data/`; 2023.

[67] Michael P Owen et al. "ACAS Xu: Integrated collision avoidance and detect and avoid capability for UAS". In: *2019 IEEE/AIAA 38th Digital Avionics Systems Conference (DASC)*. IEEE. 2019, pp. 1–10.

[68] Mark Paster. "Hydrogen deliver options and issues". In: *United States Department of* (2006).

[69] "PEM Fuell Cell MODEL for Conceptual Design of Hydrogen eVTOL Aircraft". In: (2021).

[70] TEAM PERSEUS and Tom Rathmes. June 2023.

[71] "Preliminary design of the superconducting rotor for nasa's high-efficiency megawatt motor". In: *2018 Joint Propulsion Conference* (2018).

[72] Dr. Werner Grimm Prof. Dr.-Ing. Walter Fichter. "Flugmechanik". In: ().

[73] KM Al-Qahtani et al. "Improved residual weighting for NLOS mitigation in TDOA-based UWB positioning systems". In: *2014 21st International Conference on Telecommunications (ICT)*. IEEE. 2014, pp. 211–215.

[74] *RAPID™ — Stratom's Autonomous Refueling, Recharging and Liquid Transfer System*. stratom. https://www.stratom.com/rapid-stratoms-autonomous-refueling-recharging-and-liquid-transfer-system/; 2023.

[75] Edward N Rappaport et al. "Advances and challenges at the National Hurricane Center". In: *Weather and Forecasting* 24.2 (2009), pp. 395–419.

[76] *Researchers develop robot for automated aircraft ground refueling*. Wright-Patterson AFB. https://www.wpafb.af.mil/News/Article-Display/Article/400661/researchers-develop-robot-for-automated-aircraft-ground-refueling/; 2009.

[77] Ayodeji Demuren Russell L. Edwards. "Regression analysis of PEM fuel cell transient response". In: (2016).

[78] "Sandwich-Leichtbauteile in Wabenbauweise". In: ().

[79] Wafaa MR Shakir. "Performance analysis of the hybrid MMW RF/FSO transmission system". In: *Wireless Personal Communications* 109.4 (2019), pp. 2199–2211.

[80] Bodong Shang et al. "Unmanned aerial vehicle meets vehicle-to-everything in secure communications". In: *IEEE Communications Magazine* 57.10 (2019), pp. 98–103.

[81] *Sichere und leichte Hochdrucktanks für Speicherung und Transport von Grünem Wasserstoff*. Fraunhofer IMWS. https://www.imws.fraunhofer.de/de/presse/pressemitteilungen/wasserstoff-hochdrucktank-1000bar-leichtbau.html; 2019.

[82] rev. Manuel Keßler Siegfried Wagner. "Hubschrauber-Aeromechanik". In: (2023).

[83] "Solid-State Battery Roadmap 2035+". In: (2022).

[84] John H Sorensen. "Hazard warning systems: Review of 20 years of progress". In: *Natural hazards review* 1.2 (2000), pp. 119–125.

[85] Yannis Spyridis et al. "Modelling and simulation of a new cooperative algorithm for UAV swarm coordination in mobile RF target tracking". In: *Simulation Modelling Practice and Theory* 107 (2021), p. 102232.

[86] *Storage transport of liquid hydrogen*. CRYOLOR. https://www.cryolor.com/sites/cryolor/files/2023-03/cryolor-lh2-brochure-03.23-sd.pdf; 2023.

[87] Prof. Dr.-Ing. Andreas Strohmayer. *Flugzeugentwurf II*.

[88] Robert M Taylor. "Capability, cognition and autonomy". In: *Proceedings of RTO Human Factors and Medicine Panel (HFM) Symposium*. 2002.

[89] "Technology Roadmap Hydrogen and Fuel Cells". In: (2015).

[90] *THE CAVORITE X5 Patented wing system enables highly efficient operational flight*. Horizon Aircraft. https://www.horizonaircraft.com/x5-aircraft/; accessed on 10.07.2023. 2023.

[91] *The Federal Ministry for Economic Affairs and Climate Action is funding a project to further develop hydrogen fuel cell technology*. DLR. https://www.dlr.de/en/latest/news/2022/02/20220404_project-to-further-develop-hydrogen-fuel-cell-technology; 2022.

[92] J Thorbeck. "Flugzeugentwurf I und II: Manuskript zur integrierten Lehrveranstaltung: Technische Universität Berlin". In: *Technische Universität Berlin* (2001).

[93] Cordy Tymstra et al. "Wildfire management in Canada: Review, challenges and opportunities". In: *Progress in Disaster Science* 5 (2020), p. 100045.

[94] "Using Supercapacitors to Improve Battery Performance". In: ().

[95] Reza Monir Vaghefi, Javier Schloemann, and R Michael Buehrer. "NLOS mitigation in TOA-based localization using semidefinite programming". In: *2013 10th Workshop on Positioning, Navigation and Communication (WPNC)*. IEEE. 2013, pp. 1–6.

[96] *Wasserstoff von der eFarm*. Spangler Automation. https://spangler-automation.de/aktuelles/archiv/newsletter-archiv/newsletter-oktober-2019/wasserstoff-von-der-efarm/; 2023.

[97] *Wasserstoffkraftwerk Rostock: Neuer Energieversorger?* NDR. https://www.ndr.de/nachrichten/mecklenburg-vorpommern/Wasserstoffkraftwerk-Rostock-Neuer-Energieversorger,wasserstoffkraftwerk html; 2020.

[98] Andrew H Weisberg et al. "Delivery of cold hydrogen in glass fiber composite pressure vessels". In: *International journal of hydrogen energy* 34.24 (2009), pp. 9773–9780.

[99] *What is GNSS RTK.* Mapscaping. https://mapscaping.com/what-is-gnss-rtk/#:~:text=RTK%20works%20by%20using%20a,calculated%20from%20the%20satellite%20signals.; accessed on 06.07.2023. 2023.

[100] *Why Predictive Maintenance in Aviation Can Save Lives.* ToolSense. https://toolsense.io/maintenance/why-predictive-maintenance-in-aviation-can-save-lives/; accessed on 09.06.2023.

[101] Karen Willcox. *Aircraft Systems Engineering Cost Analysis.* 2004.

[102] T Wittmann et al. "DIE LUFTVERSORGUNG VON PEM-BRENNSTOFFZELLEN IN GROSSEN FLUGHÖHEN". In: ().

[103] Sheng Xu, Kutluyil Doğançay, and Hatem Hmam. "Distributed path optimization of multiple UAVs for AOA target localization". In: *2016 IEEE International Conference on Acoustics, Speech and Signal Processing (ICASSP).* IEEE. 2016, pp. 3141–3145.

[104] Jawad N Yasin et al. "Unmanned aerial vehicles (uavs): Collision avoidance systems and approaches". In: *IEEE access* 8 (2020), pp. 105139–105155.

[105] CHEN Zhenli et al. "Assessment on critical technologies for conceptual design of blended-wing-body civil aircraft". In: *Chinese Journal of Aeronautics* 32.8 (2019), pp. 1797–1827.